Charles University in Prague

Faculty of Mathematics and Physics

Diploma thesis

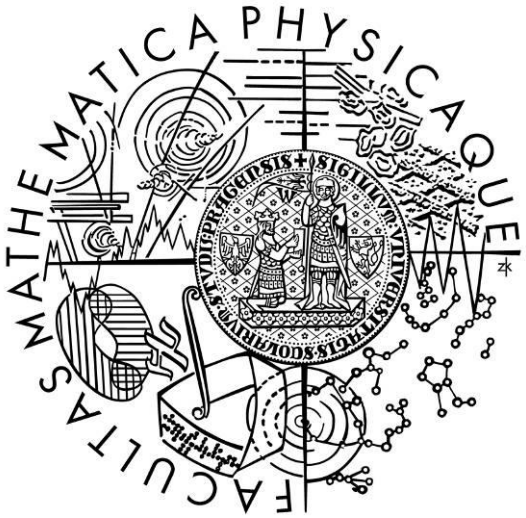

Peter Minárik

Effect of microstructure on mechanisms of plastic deformation in fine-grained magnesium alloys

Department of Physics of Materials

Supervisor: Dr. rer. nat. Robert Král, Dr.

Study program: Physics, Physics of Condensed Systems and Materials

2010

This way I would like to thank Dr. rer. nat. Robert Král, Dr. for his skilled supervision and many constructive comments.

Likewise I would like to thank Doc. RNDr. Miloš Janeček, CSc., Ing. Michal Bukovina, Ing. Viktor Škorík, Mrs. Marta Čepová and Ing. Jiří Macl for their priceless help through the measurements.

Hereby I declare that I wrote this thesis myself with the help of no more than the mentioned literature. I agree with lending and publication of this thesis.

In Prague, 15.04.2010 …….

Peter Minárik

Table of contents

Názov práce: Vplyv mikroštruktúry na mechanizmy plastickej deformácie v jemnozrnných horčíkových zliatinách

Autor: Peter Minárik

Katedra: Katedra fyziky materiálů

Vedúci diplomovej práce: Dr. rer. nat. Robert Král, Dr.

e-mail vedúceho: rkral@met.mff.cuni.cz

Abstrakt: Táto práca sa zaoberá štúdiom vplyvu zjemnenia zrna na mechanické vlastnosti a koroziodolnosť horčíkových zliatin potenciálnych pre použitie v medicíne – AE21 a AE42. Mechanické vlastnosti sa menili s pretláčaním cez ECAP v súlade s literárnymi zdrojmi. Zmenšením zrna bola získaná zvýšená koroziodolnosť v zliatine AE42. Korózna vrstva, vytvorená na povrchu, bola ďalej študovaná pomocou svetelnej a elektronovej mikroskopie. Taktiež bol študovaný efekt veľkosti zrna na charakter koróznej vrstvy. Zliatina AE42 je perspektívna na ďalšie štúdium v oblasti materiálov potenciálnych pre medicínu. Zliatina AE21 bola vylúčená z ďalších štúdií kvôli vysokej korozivite, dokonca aj po pretlačení cez ECAP.

Kľúčové slová: horčík, zliatina, koroziodolnosť, zrno, korózna vrstva, mikroštruktúra

Title: Effect of microstructure on mechanisms of plastic deformation in fine-grained magnesium alloys

Author: Peter Minárik

Department: Department of Physics of Materials

Supervisor: Dr. rer. nat. Robert Král, Dr.

Supervisor's e-mail: rkral@met.mff.cuni.cz

Abstract: In this work were studied effects of the grain refinement on the mechanical properties and the corrosion resistance of magnesium alloys potential for medical applications – AE21 and AE42. Mechanical properties changed after ECAP pressing in consistency with literature data. Enhanced corrosion resistance in AE42 alloy was achieved by the grain refinement. Corrosion layer created on the surface was observed by light and electron microscopy. Effect of the grain size on the character of the corrosion layer was investigated. AE42 alloy is suitable for further investigation as potential biodegradable material. AE21 alloy was excluded from further investigation due to low corrosion resistance even after ECAP treatment.

Keywords: magnesium, alloy, corrosion resistance, grain, corrosion layer, microstructure

1 Introduction

1.1 General information

In past few decades, there is noted a growing demand for a strong and lightweight material mainly in automobile and aerospace industry, where the operating costs highly depend on used material. At present time, the most used ultra-lightweight materials are various aluminium alloys with addition of alloying elements such as silicon, copper, magnesium, zinc, etc. When there is a higher need for mechanical strength, titanium is used.

Magnesium became very attractive material because it is the lightest structural material on Earth with the density 1.74 $kg.dm^{-3}$ (density of aluminium is 2.7 $kg.dm^{-3}$ and titanium 4.5 $kg.dm^{-3}$). There are many negative properties of the pure magnesium, therefore magnesium alloys are used in a greater scale. Magnesium and magnesium alloys have many advantages such as high specific strength, good castability (suitable for high pressure die-casting), ability to be turned/milled at high speed and good weldability under controlled atmosphere. Also relative low production cost, high recycling ability and good dumping properties are worth mentioning. The main disadvantages are low elastic modulus, limited cold working and toughness, limited strength and creep resistance at elevated temperatures, high degree of shrinkage on solidification, high chemical reactivity and in some applications limited corrosion resistance [1].

Magnesium and magnesium alloys are increasingly used in automotive industry because of properties mentioned above, especially high strength to weight ratio. Recently numerous researchers had focused on biocompatibility and biodegradability of magnesium and several works revealed promising application in the medicine. At present time is research oriented mainly on a coronary stents [2] and a bone fracture fixation implants, mostly due to their high specific strength and elastic modulus similar to bone tissue [3]. Coronary stents are being implanted to patients under clinical trials, but there are still many problems that have not been solved yet. However application as fracture fixations is limited due to problems connected with their ductility during production, corrosion resistance and non-toxicity. Many efforts have been made to develop new alloys and optimization of treatment technology to obtain high quality product, which could compete with other structural materials. The most popular magnesium alloys in automotive industry are so-called AZ and AM type alloys, where the main elements besides magnesium are aluminium (A), zinc (Z) and manganese (M). Their success is based on excellent combination of mechanical strength, castability and ductility. Another perspective alloys are AE type alloys, where E means rare earth element, which are regarded as promising in the medicine applications [4]. But application in this area is still limited mainly due to poor plasticity and corrosion resistance.

Several researchers have presented, that mechanical properties of magnesium alloys could by considerably improved by achieving an ultra-fine grain (UFG) structure [5, 6]. Also it was shown that AZ31 alloy gained better corrosion resistance in salt solution after obtaining this structure [7], what leads to other technical applications and opens a new direction of researching other ways of the corrosion resistance improvement of magnesium alloys. Over last decade there

has been notable interest in the material development area in investigation and characterization of UFG materials. The interest is stimulated mainly due to their unique microstructure and excellent mechanical properties what predicts these materials for many construction applications. Their mechanical strength is often 2-3 times higher than the strength of materials with large grains ($d > 50\mu m$), with the same or better workability after additional grain refinement. Nowadays there can be found many new technologies of UFG materials preparation such as equal channel angular pressing (ECAP) [8], high pressure torsion (HPT) [9], accumulative roll bonding (ARB) [10], inert gas condensation [11] and high energy ball milling [12]. ECAP, first reported by Segal [8], belongs to the most popular preparation method of the bulk UFG materials. Bar shaped specimen is machined to fit into a channel contained within a die and is pressed through the die using plunger. Shear deformation is introduced into the specimen because of the shape of the channel which is generally bent at the angle equal or very close to 90°. An equivalent strain of about 1 is achieved in this configuration of the die. Since the cross-section of the specimen after pressing is unchanged, it can undergo repeated pressing to obtain high degree of strain [13]. Also the specimen can be rotated between subsequent pressings and therefore different structures can be obtained. ECAP is an attractive process because it can be easily scaled up to prepare larger specimens [14]. Another benefit of ECAP process is the possibility to change the texture of the material. The < a > basal slip and the {11-20} twinning operate during the room temperature deformation of magnesium alloys. The activation of other slip systems is quite difficult, but the ECAP can change the structure of the specimen, facilitating the non-basal slip and thus enhance the ductility [15]. Structure change due to/after ECAP processing highly depends on material, strain introduced (number of routes), temperature, processing rate, stress, route changes and other conditions. Despite of large number of experiments there is no general rule to obtain optimal grain refinement or mechanical properties improvement [16]. Recently there was proposed a two steps treatment system by Horita, including initial extrusion and consequent ECAP processing. This process was specified as EX-ECAP and was successfully used in obtaining bulk UFG microstructure in many materials. In several magnesium alloys there was achieved improved ductility or even superplasticity [17, 18].

Another forming process, originally used to cross-section reduction of bars and pipes in many industry applications, is rotary swaging [19]. Recently this process came in focus because it provides ability to process pure magnesium and magnesium alloys more efficient than simple die-casting and extrusion [20]. Main reason is lower temperature and bigger velocity of processing in contrast with extrusion [21, 22]. Here can be achieved even finer microstructure by optimizing rotary swaging processing conditions (temperature, feed velocity) than by direct, eventually indirect extrusion [23].

Application of magnesium and its alloys in medicine and optimizing of their properties have a long tradition. Almost 70 years ago there were performed first attempts of using magnesium alloys as implants without negative reaction observation near implants surrounding [24-26]. Recently there were published positive effects of magnesium alloys with aluminium addition and/or lithium and rare earth elements on bone growth [27]. AE21 alloy is currently used most often [2].

1.2 Biodegradability

Metallic implants have major role as biomaterials to assist with reparation or replacement of bone tissue which is damaged or diseased. There are three main categories of metallic implants used these days: stainless steel, titanium and cobalt-chromium based alloys. There are several limitations in the application of these materials, such as possibility of release toxic ions and/or particles through corrosion and wear process. Elastic modulus of current metallic implants is quite different than a bone structure, what leads to stress shielding effects, what can reduce the bone growth stimulation. Because current metallic implants are neutral in the human body, there is necessitate of second operation after bone recovery to remove the implant and so prevent pain, accumulation of the metal in the tissue, corrosion etc. This operation presents a risk of additional infection or other complications. It takes place after the healing process is completed so it prolongs overall recovery [28]. These problems can be solved by application of biodegradable materials. The main idea is that after the bone is healed, the implant with no additional use will decompose in the body.

Current biodegradable synthetic polymer implants have inadequate mechanical properties. Magnesium and its alloys are considered as a new course in this area of research due to their several biological qualities. The leading characteristic is that metallic magnesium and its alloys are biodegradable in body fluids by corrosion and Mg^{2+} is harmless to human body. Mechanical properties make them very attractive for bone repairing because elastic modulus, density and yield strength are closer to the bone tissue than that of conventional implants [29]. Problem of magnesium alloys, that has to be figured before application of this material in wider scale, is rapid corrosion. There is high possibility of losing mechanical properties before healing process is finished. A possible way to slow down biodegradation rate of magnesium alloys is a surface treatment such as fluoride conversion coating [30], alkali heat treatment [31], hydroxyapatit coating [29] and plasma immersion ion implantation [32].

Nevertheless, surface treatment of final product will slow down the corrosion rate only temporarily and after degradation of surface layer rapid corrosion takes place again. Besides the potentially harmful corrosion products and decrease in strength of the implant, the degradation process of magnesium in human body is accompanied by hydrogen development that can be serious in higher corrosion rates. Although the most important role plays the chemical and phase composition of the alloy. The corrosion resistance can be also substantially increased by suitable microstructure, namely ultra-fine grain structure [7].

1.3 Material characteristic

It can be considered that biomaterial that will decompose in a human body should contain in higher concentrations only elements which occur in the body naturally. From this reason, magnesium alloys are perspective to be used as biodegradable materials and there are published numerous works, that alloys containing rare earth elements owns best qualities in this area [2, 4,

27, 33]. One of the first studies with magnesium based implants were performed by Heublein et al., who implanted stents made from AE21 alloy into a pig with 50% loss of mass within six months [4].

AE21 alloy contains 2% aluminium atoms and 1% rare earth (RE) elements (Ce, Nd, La, etc.), besides magnesium. It was derived from commercial creep resistant alloy AE42 containing double number of alloying elements. A casting magnesium alloy AE42 was developed for high temperature application. Typical microstructure of Mg-Al alloys is composed of α-Mg matrix and $Mg_{17}Al_{12}$ precipitations but due to instability of β-$Mg_{17}Al_{12}$ phase the application of magnesium alloys is restricted for temperatures above 120 °C [34-37]. Aluminium is added to AE42 alloy to improve castability and room temperature mechanical properties and RE are added for creep resistance [38]. Lamellar $AL_{11}RE_3$ phase, which dominates interdendric microstructure, appears to be critical for the creep resistance below 150 °C. Above this temperature $Al_{11}RE_3$ diminishes in volume fraction, and concurrent formation of $Mg_{17}Al_{12}$ phase takes place what deteriorates creep resistance [39].

1.4 Grain boundary strengthening

Mechanical strength of metallic materials depends on mobility of dislocations. More easily dislocations can spread through the material; less stress needs to be applied to deform it. Propagation of dislocations is limited by pinning points that halt dislocation movement and therefore there is need for greater amount of force to be applied to overcome the barrier. Most usual pinning points are point defects, alloying elements, second phase precipitates and grain boundaries. In polycrystalline metals grain boundaries take significant part in strengthening of the material. As mentioned above, grain boundaries limit the motion of dislocations due to the fact that the dislocations have to change direction when entering adjacent grain and also because grain boundaries are much more disordered than grains inners. When metal is deformed, existing dislocations and created dislocations start to move until they reach grain boundary. At this point pile-up is created at grain boundary and all dislocations affect with their stress fields the dislocation nearest to the grain boundary, so it is forced to cross into next grain by external stress and stress from surrounding dislocations. When grain structure became finer, fewer dislocations are able to occur in grains and therefore there is need for greater amount of external stress to be applied to compensate stress field from missing dislocation. The dependence of mechanical strength on a grain size of polycrystalline metals is described by Hall – Petch equation given by (1), where σ_0 is the friction stress in the absence of grain boundaries, k is a constant and d is the grain size.

$$\sigma_y = \sigma_0 + kd^{-1/2} \tag{1}$$

If there were not any limitations, mechanical strength would rise to infinity with decreasing of grain size. But it is observed that under certain critical value of the grain size, metal softening

occurs. It is called the inverse Hall – Petch relation and although this phenomenon is not clearly identified yet, there are numerous studies bringing light into this problem [40-45].

1.5 ECAP and microstructural development

As mentioned in introduction EACP is one of the most developed methods to prepare bulk UFG materials. Because of unchanged cross-section the billets can undergo several passes. During repetitive pressings, the shear strain is accumulated in the billet, leading ultimately to a UFG structure. In practice, different slip systems may be introduced by rotating the billet about its longitudinal axis between each pass and this leads to four basic processing routes: there is no rotation of the billet in route A, rotations by 90° in alternate directions or the same direction in routes B_A and B_C, respectively, and rotations by 180° in route C. When using a die with a channel angle of $\Phi = 90°$, route B_C is generally the most expeditious way to develop a UFG structure consisting of homogeneous and equiaxed grains with grain boundaries having high angles of misorientation [46]. On Figure 1 (a) is presented graphical description of types of the routs and on Figure 1 (b) are presented slip systems that are activated in each route.

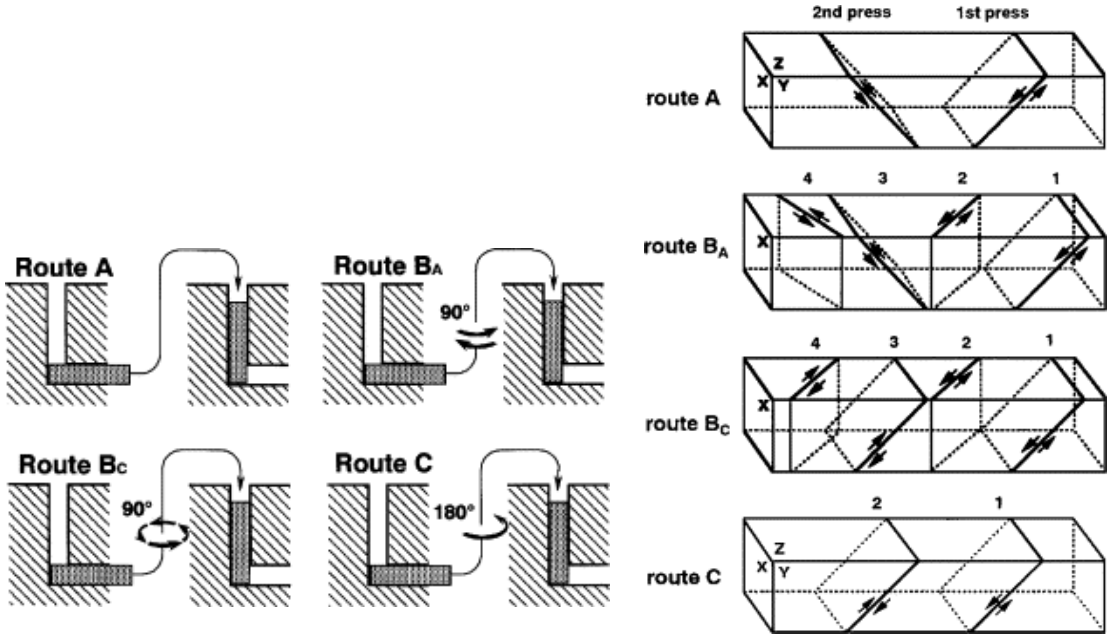

(a) (b)

Figure 1: Graphical description of (a) types of routs [47], (b) activated slip systems [48]

As presented in [49], the microstructure of the specimen after ECAP pressing, following the route B_C changes. Besides grain refinement also alternation of the texture was observed. The texture with basal poles oriented mainly towards the pressing direction created by prior extrusion was continuously changed by more ECAP routs. After the first pressing a new component of the texture was inclined by about 40° relatively from the initial orientation and after 12 passes became the major texture component.

1.6 Corrosion

Most metals and alloys used in a daily life change their chemical and mechanical properties in environment such as air, water, seawater etc. Almost all metals found in nature are in form of oxides, hydroxides, sulphides etc. so when a pure metal is prepared, a lot of energy is stored within it. The only exceptions are gold and platinum, which are already in the metallic form. From thermodynamic perspective there is a force that makes metals to lose this energy. This is allowed through a corrosion process. Corrosion is in the most common way known as an electrochemical oxidation of metals in reaction with an oxidant such oxygen. Speed of corrosion depends on many parameters such as composition of the metal and its surroundings, temperature, presence of radiation etc. Corrosion in an aqueous solution is the most common of all corrosion processes.

When a metal is immersed in the solution, there must be an anode, a cathode and as well an ionic and an electrical current path between them two in order to form an electrochemical process. At the anode an oxidation process takes place. In case of the metal oxidation, metal atoms lose electrons which are transferred into the metal. At the same time a reduction process of cations from the solution takes place on the cathode. Electrons flow from the anode to the cathode through the electrical path mentioned above. When the metal is homogenous the oxidation and the reduction processes can be found at the same place [50-52].

2 Experimental methods

2.1 Mechanical properties

Mechanical properties such as tensile strength, plasticity and strain rate sensitivity index were investigated by tensile deformation tests. Deformation tests were performed by the deformation device INSTRON 5882 equipped with a thermal regulated oven and controlled by a computer by the Bluehill program.

2.1.1 Tensile strength tests

Tensile strength tests provided a time vs. applied force characteristics. From a known movement rate of the device a tensile strain of the specimen was determined. The tensile strain contained two components: an elastic strain of a specimen and the device and a plastic strain of the specimen. The elastic strain part was subtracted during measurement evaluation. The elastic region of the applied force vs. tensile strain plot was interpolated by a line in the area of maximum of the first derivative of the applied force with respect to the tensile strain. True strain of the specimen was determined as:

$$\varepsilon = ln\left(1 + \frac{dl_{pl}}{l_0}\right) \tag{2}$$

And true stress in specimen as:

$$\sigma = \frac{F}{S_0} ln\left(1 + \frac{dl_{pl}}{l_0}\right) \tag{3}$$

where

$$dl_{pl} = vt - \frac{F - b_0}{b_1} \tag{4}$$

F represents the applied force on the specimen, S_0 initial cross section of the specimen, l_0 initial length of the specimen, v movement rate of the device, t time and b_0 and b_1 are coefficients of the line, which interpolated the linear part of the applied force vs. extension plot.

2.1.2 Strain rate sensitivity index *m*

The high strain rate sensitivity of the flow stress, which is quantitatively certified by the value of the strain rate sensitivity index m, is believed to be the most important mechanical characteristic of superplastic material. Superplastic materials are polycrystalline solids that are able to undergo large uniform strain before failure. The mechanical behaviour of superplastic material is often described as:

$$\dot{\varepsilon} = C\sigma^{\frac{1}{m}} \tag{5}$$

The value of m does not exceed usually 0.1 for the most of known polycrystalline materials. However, for the materials in the superplastic state the value of *m* commonly lay in the range 0.3 to 0.9 [53]. Values of strain rate sensitivity index *m* were determined by (6) during step strain rate tests at constant temperature.

$$m = \frac{log(^{\sigma_2}/_{\sigma_1})}{log(^{\dot{\varepsilon}_2}/_{\dot{\varepsilon}_1})} \tag{6}$$

2.2 Corrosion

Electrochemical corrosion characteristics of studied specimens were obtained by electrochemical impedance spectroscopy and potentiodynamic tests. Characteristics were measured by a computer by a VoltaMaster 4 program using a potentiostat/galvanostat Voltlab PGZ100 and a three electrodes set-up. Also immersion corrosion tests were performed to study stability of the corrosion layer and its microstructure.

2.2.1 Potentiodynamic tests

The potentiodynamic (PD) test is a method used for acquiring an electrical current density as a function of a potential. To acquire this functionality the potential of a specimen have to be shifted anodic (eventually cathodic) side, where an anodic reaction is preferred and therefore corrosion is favoured. From measured data a corrosion potential and a corrosion current density can be calculated.

The electrical current represents the rate with which the anodic and the cathodic reactions take place on the surface of the specimen. In general the anodic current is considered to be positive and the cathodic negative. When immersed specimen is in balance with its surroundings, the potential against reference electrode is being settled. This potential is called the corrosion potential and its value characterizes the potential when the anodic and the cathodic currents are equal. Value of the anodic/cathodic current is value of the corrosion current and typically is expressed as a current per working area of the electrode (specimen). By shifting the potential, a driving force available for reactions on the surface is being changed. This results to indirect control of the reactions rates on the specimen-electrolyte interface. A potentiostat is used to change the potential and to measure the current, which is applied to achieve the desired degree of polarization.

Measured data are plotted in an Evans diagram (a plot of *E* vs. *log(I)*) where absolute value of the current density is plotted and the data are evaluated by the Tafel's analysis. The tafel slopes b_a (anodic reaction) and b_c (cathodic reaction) may be obtained from the linear regions of the polarization curve as illustrated in Figure 2. A point where these slopes cross is the point of the corrosion potential and the corrosion current density [50, 51].

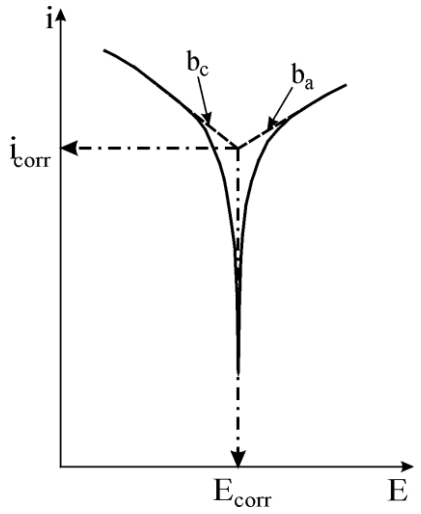

Figure 2: The Tafel's analysis of the PD test

2.2.2 Electrochemical impedance spectroscopy

The PD test is useful method when the specimen with initial surface conditions is about to be measured, but when a non-conducting layer is created on the surface, this method provides solid data no more. The electrochemical impedance spectroscopy (EIS) can be used even when the layer is created. In contrast to the PD test, AC potential is being applied to an electrochemical cell and an electrochemical impedance of the cell is being measured. A current frequency is being changed through experiment in successive steps, from hundreds of kHz to mHz and the complex impedance is set for every value. If the real part of the impedance is plotted on the X-axis and the negative imaginary part is plotted on the Y-axis, a "Nyquist Plot" is obtained (Figure 3), what is a general data representation for this method. For measured data evaluation is important to determine an equivalent circuit of specimen-electrolyte interface which usually consist of an electrolyte resistance, a polarization resistance and a capacitance of a double layer, made by the non-conductive layer on the surface. The most common Nyquist Plot shape is a semicircle which is characteristic for the simple equivalent circuit shown on Figure 4.

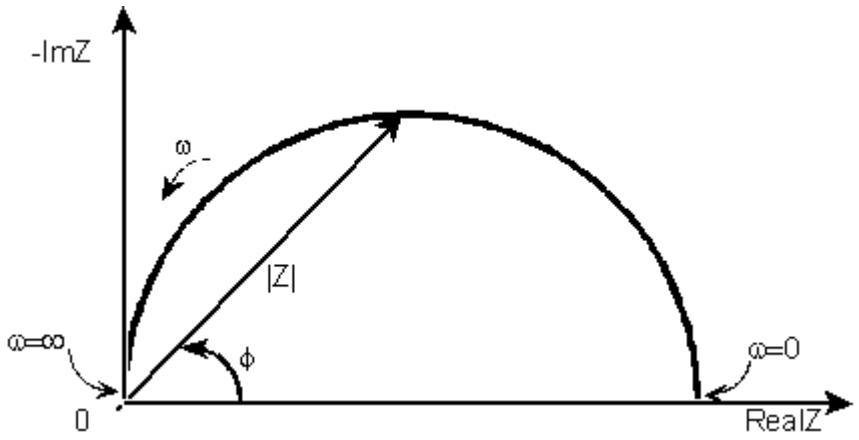

Figure 3: The Nyquist Plot for the simple equivalent circuit with an impedance vector

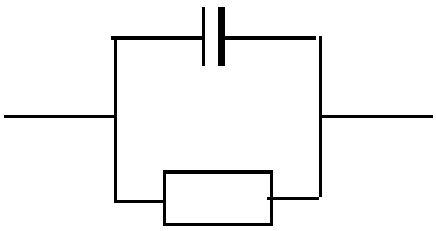

Figure 4: The simple equivalent circuit

The equation of the simple equivalent circle shown on Figure 4 is:

$$Z = R_\Omega + \frac{R_p}{1+j\omega CR_p} \tag{7}$$

For $\omega \to 0$ holds:

$$R_\Omega + R_p = \lim_{\omega \to 0} Z \tag{8}$$

And for $\omega \to \infty$ holds:

$$R_\Omega = \lim_{\omega \to \infty} Z \tag{9}$$

The real and the imaginary part of the impedance (7) are defined as:

$$Z_r = R_\Omega + \frac{R_p}{1+(\omega CR_p)^2} \tag{10}$$

$$Z_i = -\frac{\omega CR_p^2}{1+(\omega CR_p)^2} \tag{11}$$

As (10) and (11) are combined, the Nyquist Plot semicircle equation with the diameter R_p is acquired:

$$\left(Z_r - R_\Omega - \frac{R_p}{2}\right)^2 + (Z_i)^2 = \left(\frac{R_p}{2}\right)^2 \tag{12}$$

In general, the impedance of the surface exhibits more complicated behaviour. This model does not take into account the time constants of adsorption phenomena and the individual reaction steps of the overall charge transfer reaction. Also surface roughness or non-uniformly distributed reaction sites lead to a dispersion of the capacitive time constants. As a consequence, in the Nyquist plot the semicircle corresponding to a charge transfer resistance in parallel to the double layer capacitance becomes flattened. The double layer capacitance is therefore replaced by constant phase element (CPE), defined as (13) where Y_0 is impedance when $\omega = 1$ rad/s and n is a coefficient.

$$Z_{CPE}(\omega) = \left(\frac{1}{Y_0(j\omega)^n}\right) \tag{13}$$

This is a general dispersion formula, for $n = 0$ it stands resistance and for $n = 1$ the frequency dependence of the CPE is that of a capacitance. In all cases of studying the corrosion resistance, n is close to 1 representing capacitive characteristic of the interfaces [51, 52, 54].

2.3 Microstructure

Microstructures of studied alloys were investigated by transmission electron microscope (TEM), scanning electron microscope (SEM) and metallographic microscopy. TEM was used to study microstructure evolution after ECAP processing and SEM and metallographic microscopy to study corrosion layers developed after corrosion immersion tests.

2.3.1 Transmission electron microscope

Microstructure development during ECAP process was studied by TEM. Each specimen was mechanically polished and afterwards ion-polished. Used transmission electron microscope was Philips CM 200. All micrographs were taken in the bright field.

2.3.2 Scanning electron microscope

Corrosion layers, developed on the specimens after immersion test, and influence of the microstructure on their development were studied by SEM. For the observation of microstructure the scanning electron microscope JOEL 50XA with a Bruker QUANTAX 200 energy dispersion microanalysis system (EDS) was used. Investigation was performed by detection of secondary electrons created after impact of a primary beam on the specimen. Composition of studied area was identified according to x-radiation created after primary beam impact.

2.3.3 Metallographic microscopy

Metallographic microscopy was used in order to observe microstructure and corrosion layer. A microstructure was revealed on the specimen's surface by etching in acid. Afterwards the surface was observed by optical microscope with CCD camera, in the computer equipped by the program Lucia from Laboratory Imaging. Used metallographic microscope was OLYMPUS IX70.

2.4 Differential scanning calorimetry

Differential scanning calorimetry (DSC) is a thermodynamic technique based on temperature difference measuring, between a specimen and a reference material, during precisely defined heating or cooling, which also enables determination of specific heat capacity and phase transition temperatures. Measurements were performed by NETZSCH DSC 404C device.

3 Experimental results

3.1 Material preparation – Extrusion & ECAP

Examined magnesium alloys AE21 and AE42 were severely deformed by ECAP to prepare bulk material with UFG structure. An ECAP die (Figure 5) was placed in a screw-driven INSTRON 1186 machine which allows maximum applicable load of 200 kN. In the ECAP die both the feed-in and exit channels are formed by hardened inlays in the non-hardened die. The inlays consist of several segments of simple shape which can be easily machined and fit into the die. The ECAP die with an ejector was used to allow pushing the specimen out of the die immediately after pressing it by a plunger from the feed-in channel to the exit channel. The main advantage of using the ejector is the shorter time the specimen is exposed to the operating temperature of the ECAP process, thus avoiding the possible microstructural changes. In both dies, the angle Θ between two intersecting channels and the corner angle Ψ are 90° and 0°, respectively. Both channels have a square cross section of 10 mm × 10 mm. The length of the exit channel was optimized to allow easier processing while maintaining the straight shape of the specimen on exit.

Figure 5: The ECAP die

Prior to ECAP the specimens were hot extruded at T = 350°C with extrusion ratio ER = 12. Specimens were machined to initial dimensions of 10 mm × 10 mm × 100 mm. Both alloys were deformed to a maximum equivalent strain of 8 (1, 2, 4 and 8 passes in case of AE21 and 8 passes in case of AE42) following route Bc. Molybdenum disulphide grease was used as a lubricant. Pressing of AE21 alloy was performed at 180°C at speed of 50 mm/min for all passes. Each number of passes of AE42 alloy was prepared differently. In Table 1 is shown manufacturing procedure of AE42-8P specimen.

Table 1: ECAP procedure of AE42 alloy

Total count of the routes	Number of the route			
	1P	2P	3P	4P-8P
8P	210°C, 10 mm/min	195°C, 20 mm/min	185°C, 20 mm/min	180°C, 20 mm/min

3.2 Mechanical properties

Mechanical properties of AE21 and AE42 alloys with various number of ECAP passes were investigated by tensile deformation tests at room temperature. Specimens were machined into the shape presented on the Figure 6 and cut into 1mm thickness along the ECAP flow plane by circular saw Struers Accutom-50, by saw disc no. 10S15.

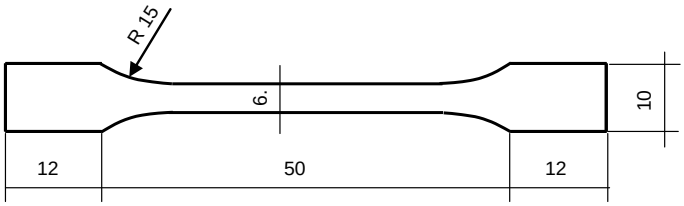

Figure 6: Schematic shape of the tensile deformation test specimens

True strain and true stress were determined according to (2) and (3) and resulting characteristics are plotted in Figure 7 and Figure 8 of AE21 and AE42 alloy, respectively.

Dependence of the yield stress at 0.2% offset strain ($\sigma_{0.2}$) on the number of ECAP passes N of AE21 alloy is presented as Figure 9. Values of $\sigma_{0.2}$ and maximum stress (σ_{max}) are presented in Table 2.

Table 2: Values of $\sigma_{0.2}$ and σ_{max} of AE alloys with various number of ECAP passes

	$\sigma_{0.2}$ [MPa]	σ_{max} [MPa]
AE42-0P	184 ± 09	309 ± 15
AE42-8P	123 ± 06	267 ± 13
AE21-0P	178 ± 09	309 ± 15
AE21-1P	210 ± 10	296 ± 15
AE21-2P	214 ± 11	296 ± 15
AE21-4P	172 ± 09	322 ± 16
AE21-8P	127 ± 06	220 ± 11

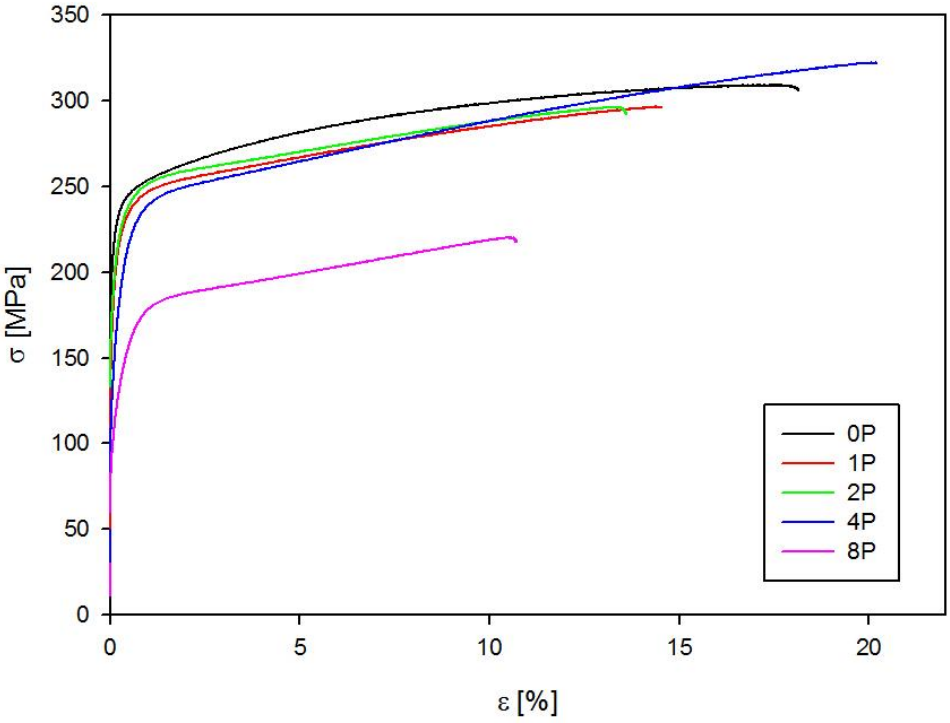

Figure 7: True stress-strain curves obtained for AE21 alloy with various number of ECAP passes

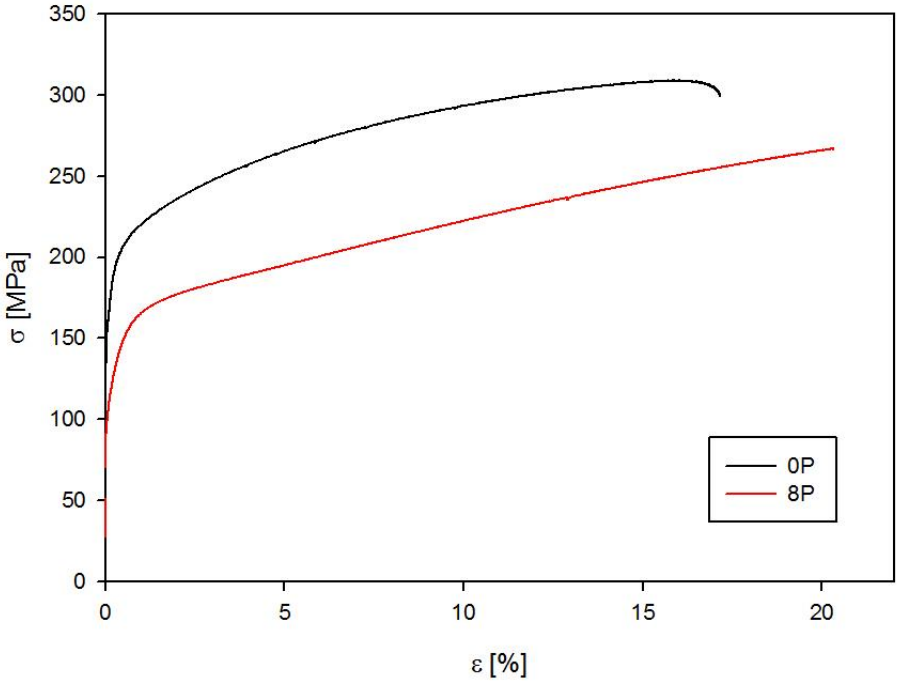

Figure 8: True stress-strain curves obtained for AE42 alloy with various number of ECAP passes

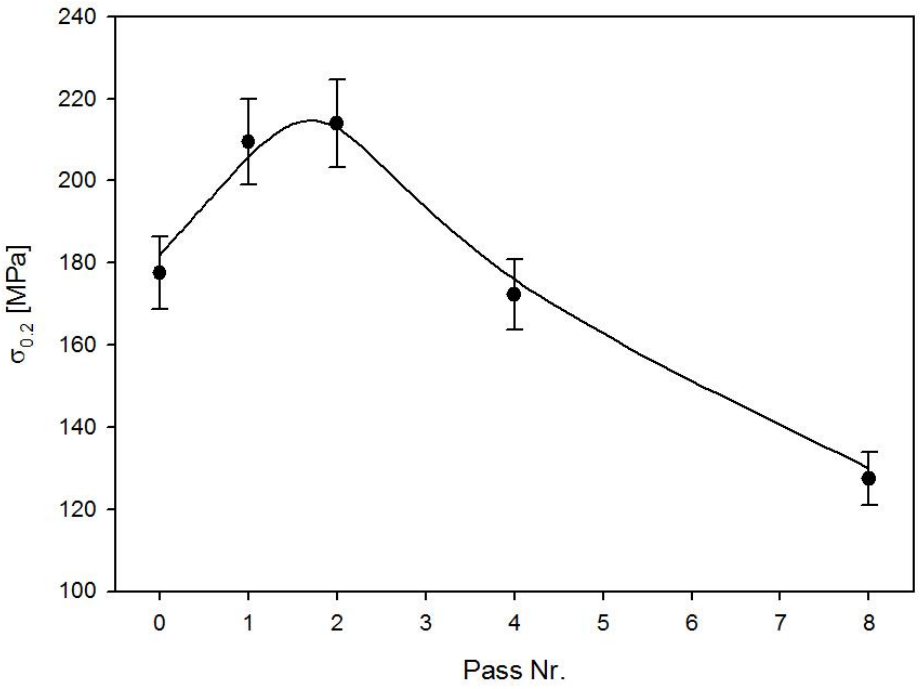

Figure 9: Dependence of the yield stress on the number of ECAP passes *N* for AE21 alloy

From Table 2 and Figures in question is apparent that the maximum stress decreased between four and eight ECAP passes but the yield strength started to decrease already after two ECAP passes. The yield stress also rose, until the second ECAP pass took place.

Values of strain rate sensitivity index *m* were determined by (6) during step strain rate tests at temperature 350°C. Temperature was measured using K-type thermocouple with possible deviation of 1°C. Specimens were placed in the oven after heating and were stabilized for 20 minutes. The strain rate was first set on 1 mm/min till 2% tensile strain was reached and then was dropped to 0.1 mm/min. The strain rate was then increased in successive steps and the corresponding steady flow stress was measured. The *m* parameter vs. strain rate characteristics are presented as Figure 10 and Figure 11 of AE21 and AE42 alloy, respectively.

As mentioned, a material can be considered as superplastic when *m* parameter is higher than 0.3. All ECAPed specimens had the best superplastic behaviour for the strain rate near to $3x10^{-4}$ s^{-1}, slowly decreasing to the higher rates. From AE21 specimens the 2P specimen was superplastic in the highest strain rates with losing this attribute approximately by $1.3x10^{-3}$ s^{-1}. AE42-8P had higher *m* parameter by all measured strain rates then AE42-0P and also higher than all AE21 specimens. Superplastic behaviour ends by strain rate approximately $1.8x10^{-3}$ s^{-1}.

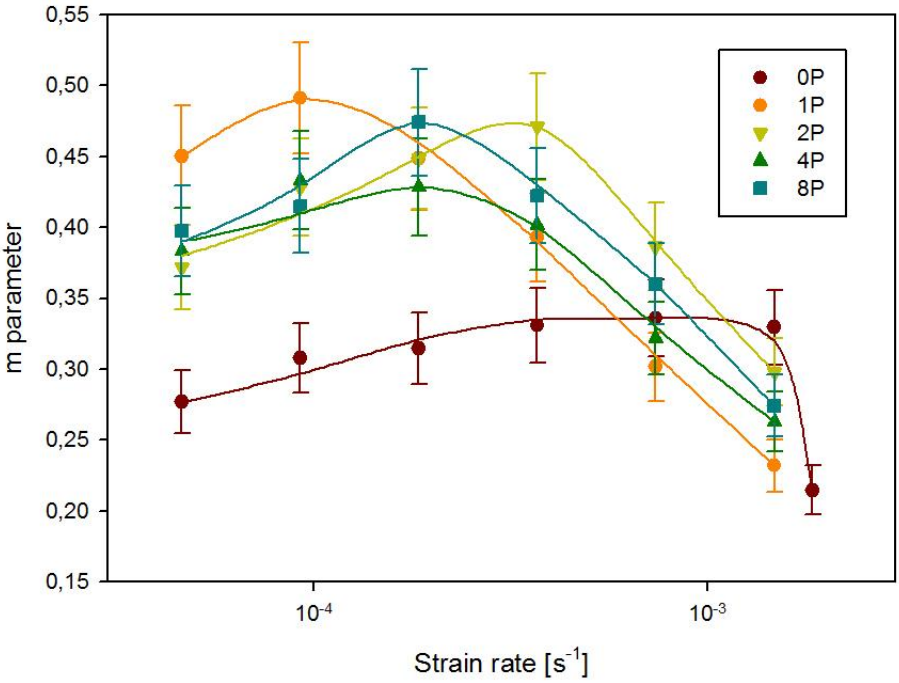

Figure 10: *m* parameter vs. strain rate characteristic of AE21 alloy with various number of ECAP passes.

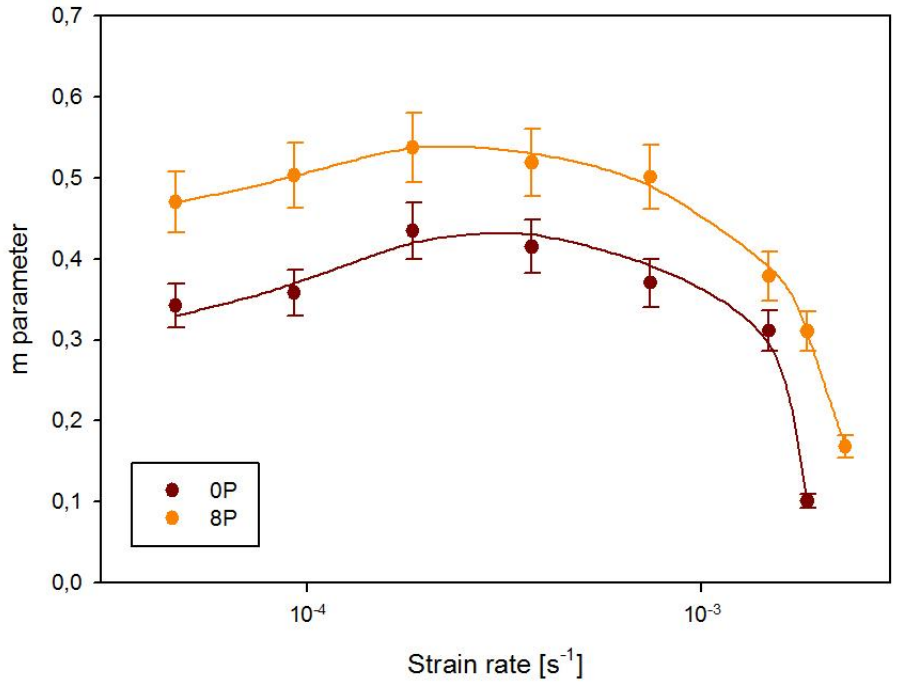

Figure 11: *m* parameter vs. strain rate characteristic of AE42 alloy with various number of ECAP passes.

3.3 Development of the microstructure of AE21 alloy

Microstructure development after ECAP pressing was studied by TEM on the extruded AE21 alloy. Specimens were cut from the middle area of the billets along the ECAP flow plane. Each was mechanically polished symmetrically from both sides by 1200 emery paper until 150 μm thicknesses was reached, and then a dimple was grinded until 20 μm thicknesses in the middle was reached. Dimples were created by Gatan DIMPLE GRINDER MODEL 656. Finally the specimens were ion-polished using Precision Ion Polishing System (PIPS) at 4 kV.

After one ECAP pressing was the microstructure highly inhomogeneous. Character of the grains/subgrains diameter was bimodal – smaller than 1 μm and between 2-3 μm. All grains/subgrains contained high number of dislocations. The present dislocation tangles were starting to form dislocation cells and subgrains as shown on Figure 12.

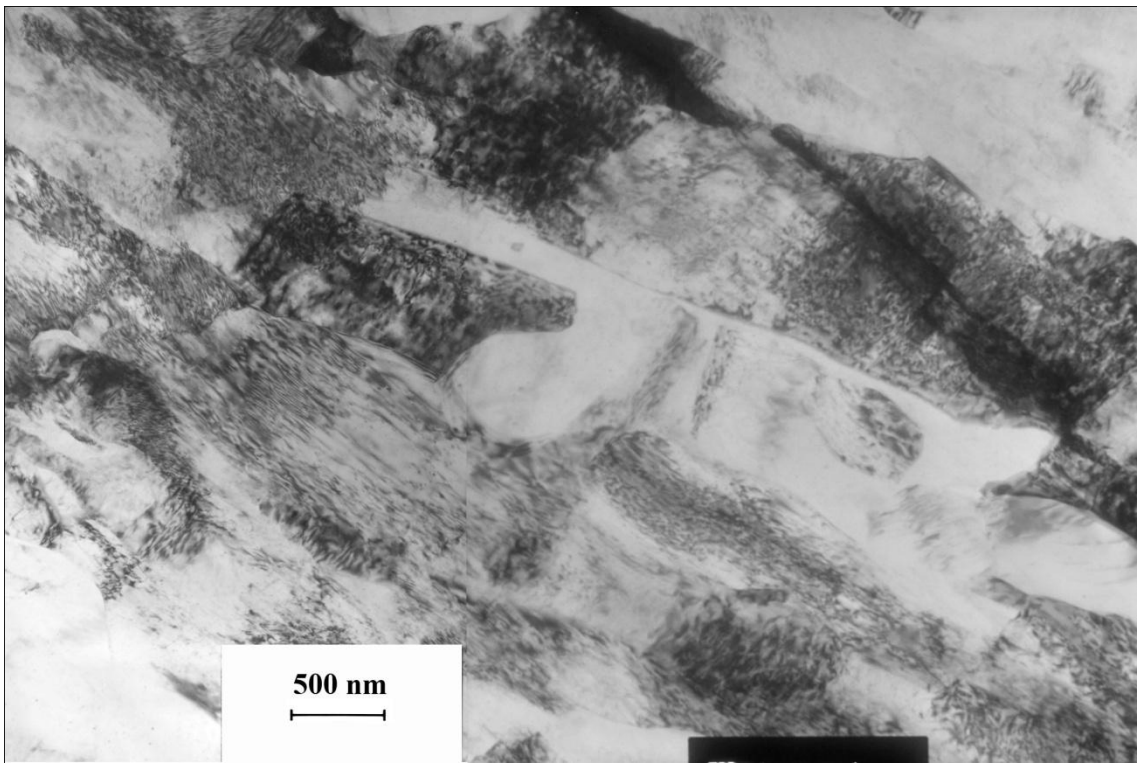

Figure 12: TEM micrograph of AE21-1P specimen – dislocation tangles

After 4P of ECAP was the microstructure still strongly deformed with high value of dislocation density. The microstructure was formed from 50-60% by dislocation tangles forming no substructure, as presented on Figure 13 (a) and from 40-50% by subgrains of average size 1 μm with high number of dislocations, as presented on Figure 13 (b). Only exceptional signs of grains with high angle grain boundaries were found, but also they contained plenty of dislocations.

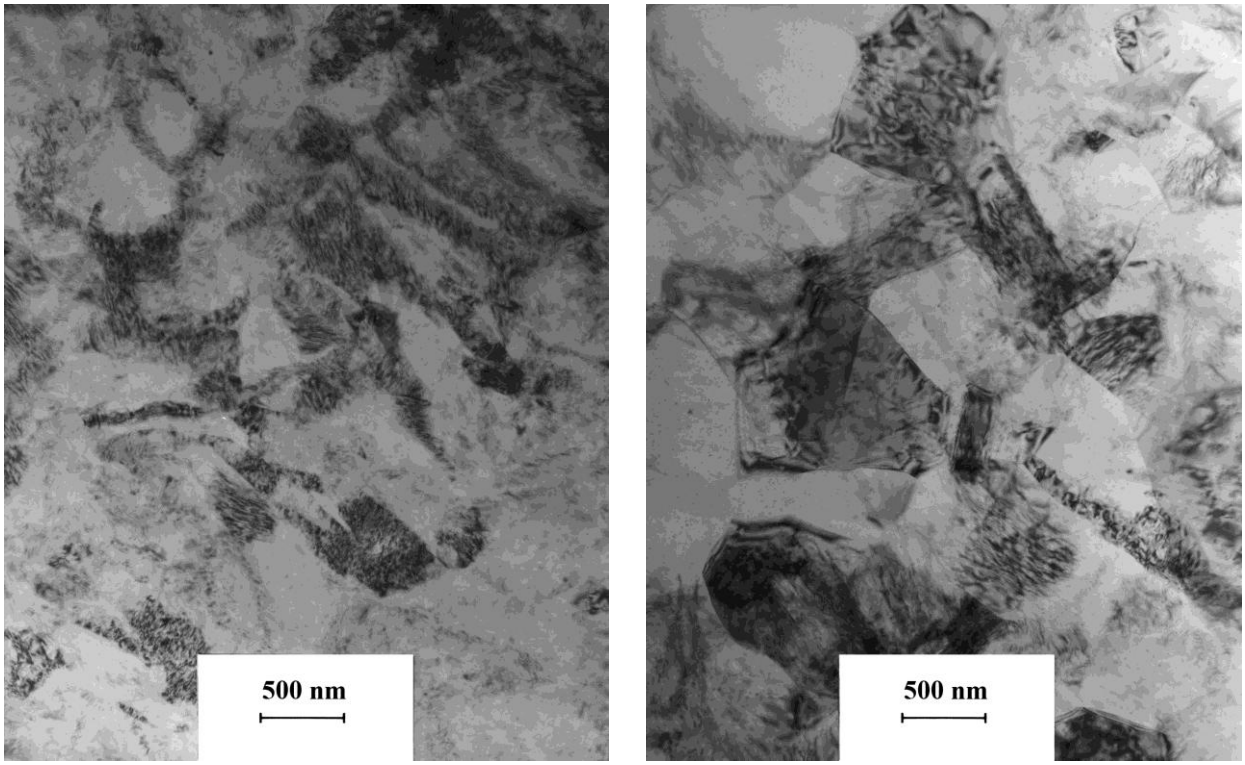

a) b)

Figure 13: TEM micrograph of AE21-4P specimen (a) dislocation tangles, (b) subgrains

The microstructure after eight ECAP pressing was formed by grains with high degree of misorientation. The structure was bimodal with grains of diameter smaller than 1 μm and of diameter between 2-3 μm. In grains it was possible to find still a lot of dislocations but there were also many grains without any dislocation with high angle grain boundaries as shown on Figure 14 (b). On Figure 14 (a) is presented micrograph with grains of different size, mostly with dislocations.

In all studied states after ECAP pressing were found also particles containing aluminium, lanthanum, cerium and neodymium. Particles were approximately 2-3 μm of the size. Micrograph of such particles found in AE21-8P specimen is displayed as Figure 15.

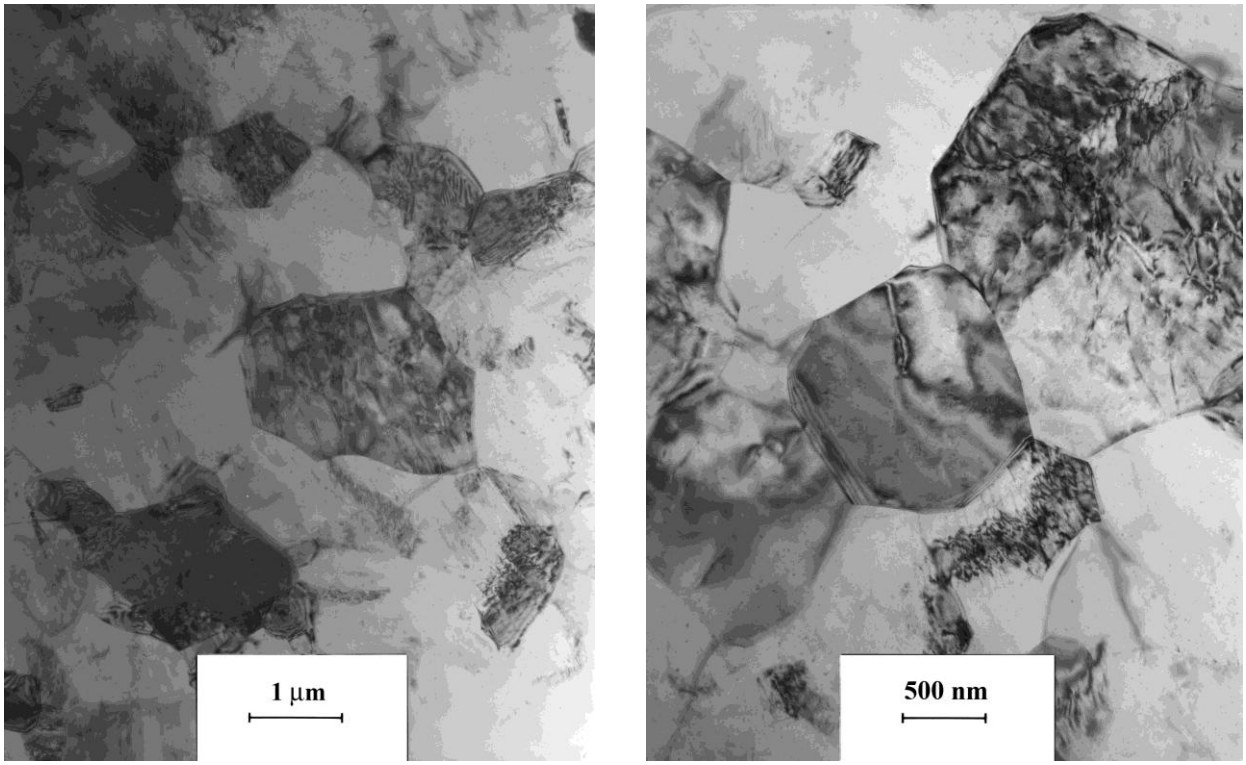

a) b)

Figure 14: TEM micrograph of AE21-8P specimen (a) grains of different size, mostly with dislocations, (b) large grains with high angle grain boundaries

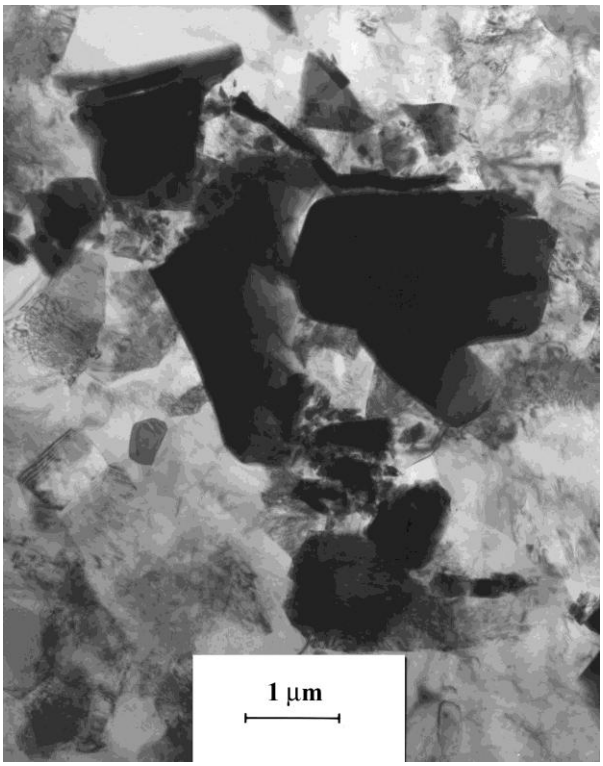

Figure 15: TEM micrograph of AE21-8P specimen – dispersed particles containing aluminium, neodymium and cerium

3.4 Electrochemical corrosion tests

To perform the PD tests was used a three electrodes set-up – the working electrode (specimen), the counter electrode and the reference electrode. The reference electrode provided a stable reference, against which applied potential was measured and the counter electrode was used to provide applied current. For the EIS test was also used the three electrodes set up, but as mentioned in section 2.2.2, an AC potential generator and a frequency analyzer was added.

Electrochemical corrosion characteristics of studied specimens, performed by EIS and PD tests, were investigated in 0.1 M NaCl solution (pH of 7 and 12). There were used the SCE (saturated calomel electrode) reference electrode and the platinum counter electrode. Addition rotation of 1000 rpm of the specimen was introduced for better homogeneity of the measurement. All specimens were cut from ECAPed billets perpendicular to the flow direction by circular saw Struers Accutom-50, by saw disc no. 10S15 and then mold into the epoxy resin. Measured surfaces of specimens were mechanically polished by 1200 emery paper and then degreased to obtain the initial surface conditions.

PD tests were performed at the room temperature from -150 mV to 300 mV with respect to the open circuit potential (OCP) after five minutes stabilization. At least three measurements were performed for each alloy in each solution. Before each measurement initial conditions of the investigated surface were obtained. Measured data were evaluated by the VoltaMaster 4 program.

Figure 16 and Figure 17 illustrate PD test characteristics of AE42 and AE21 alloys with various number of ECAP passes. All tests were performed in the corrosion solution of 0.1 M NaCl electrolyte with the pH of 7 and 12. In Table 3 and 4 are presented measured data of electrochemical characteristics acquired by Tafel's analysis, as mentioned in section 2.2.1.

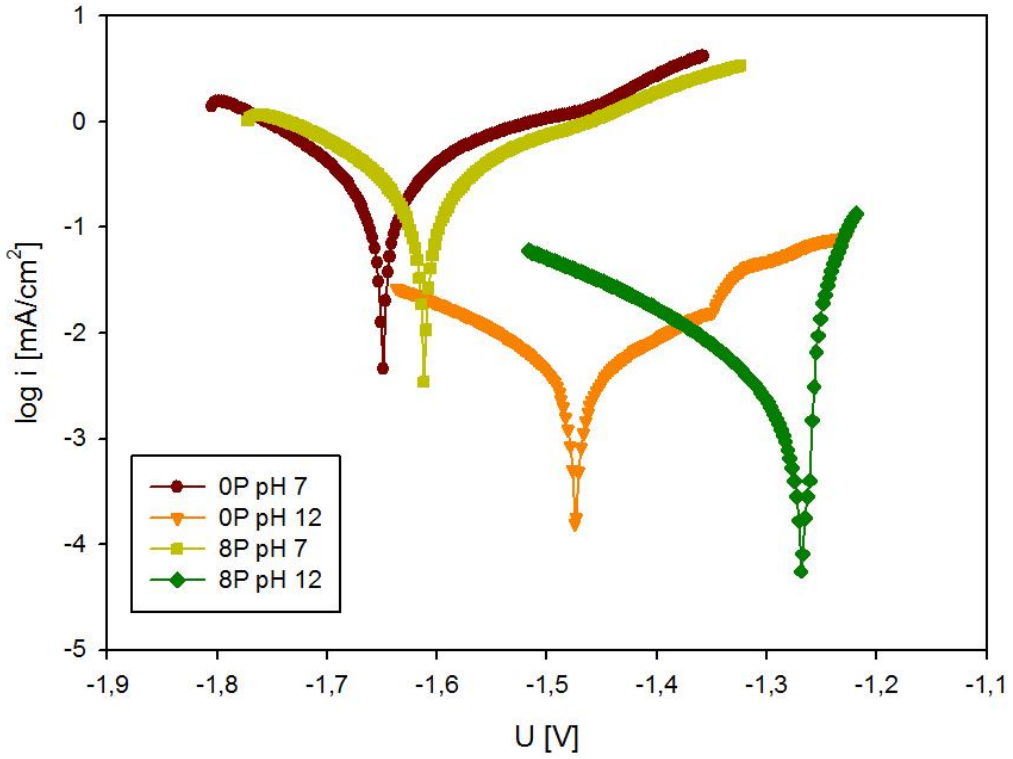

Figure 16: PD test of AE42 with various number of ECAP passes in the pH of 7 and 12

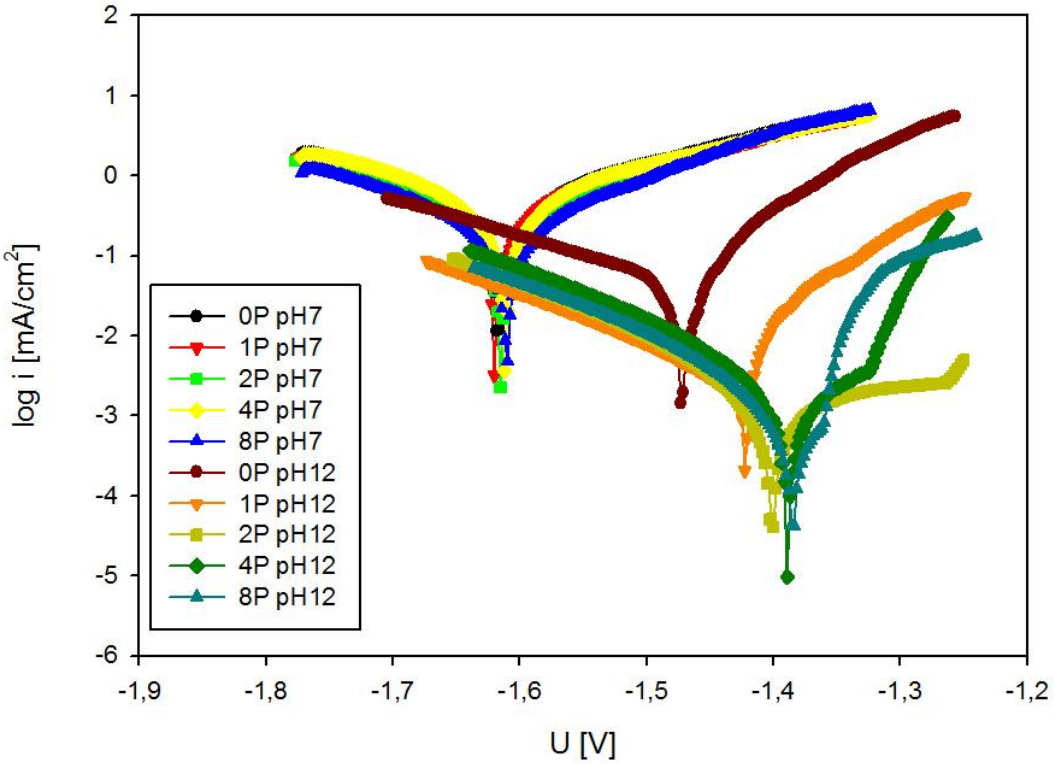

Figure 17: PD test of AE21 with various number of ECAP passes in the pH of 7 and 12

Table 3: Average values of E_{cor} [V] of AE alloys with various number of ECAP passes in the electrolyte with the pH of 7 and 12

	7 pH	12 pH
AE42-0P	-1.654 ± 0.001	-1.493 ± 0.021
AE42-8P	-1.620 ± 0.004	-1.269 ± 0.003
AE21-0P	-1.623 ± 0.004	-1.484 ± 0.014
AE21-1P	-1.625 ± 0.002	-1.450 ± 0.013
AE21-2P	-1.619 ± 0.000	-1.413 ± 0.012
AE21-4P	-1.617 ± 0.001	-1.383 ± 0.004
AE21-8P	-1.616 ± 0.001	-1.373 ± 0.012

Table 4: Average values of i_{cor} [μA/cm] of AE alloys with various number of ECAP passes in the electrolyte with the pH of 7 and 12

	7 pH	12 pH
AE42-0P	307 ± 52	5.75 ± 0.03
AE42-8P	293 ± 52	3.10 ± 0.69
AE21-0P	503 ± 19	26 ± 16
AE21-1P	378 ± 09	3.92 ± 0.93
AE21-2P	209 ± 29	3.57 ± 0.09
AE21-4P	488 ± 10	3.12 ± 0.01
AE21-8P	201 ± 32	2.74 ± 1.28

In Tables 3, 4 and in corresponding Figures can be seen a shift of E_{cor} to less negative values by higher value of the pH and also by higher number of ECAP passes. The higher value of the pH also substantially decreases i_{cor}. In characteristics measured in the pH of 12 of AE42-0P, AE21-2, 4 and 8P, when the potential reaches a sufficiently positive value the applied current rapidly increases (Figures 16 and 17).

EIS tests were also executed at room temperature after five minutes stabilization process from 100 kHz to 20 mHz with 10 mV amplitude with respect to the OCP. Also at least three measures were performed for each alloy and in each solution. Before each measurement initial conditions of the investigated surface were obtained. Measured data of EIS tests were evaluated by an EC-Lab program.

Figure 18 and Figure 19 present Nyquist plots of AE42 as extruded and after eight ECAP passes in the solution with the pH of 7 and 12, respectively. Figure 20 shows Nyquist plots after OCP stabilization in the electrolyte with the pH of 7 for 168 hours. Tests were performed in the same solutions in which specimens were immersed. Final pH of the solutions was determined as 10.2 – 10.5 for all specimens. Figure 21 and Figure 22 illustrate Nyquist plots of AE21 with various number of ECAP passes in the solution with a pH of 7 and 12, respectively.

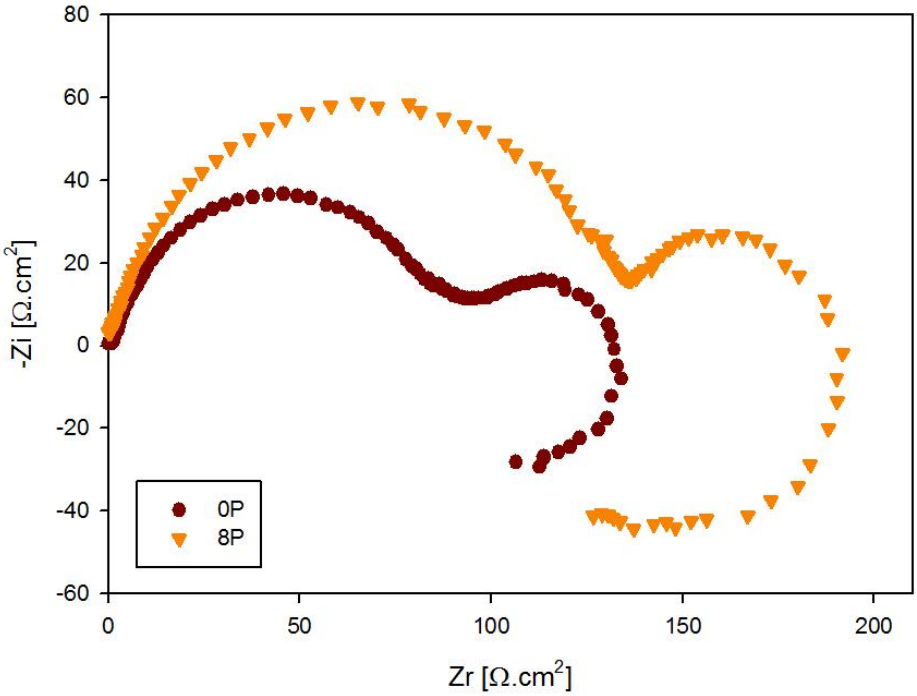

Figure 18: EIS characteristics of AE42 alloy, as extruded and ECAPed, in the solution with the pH of 7

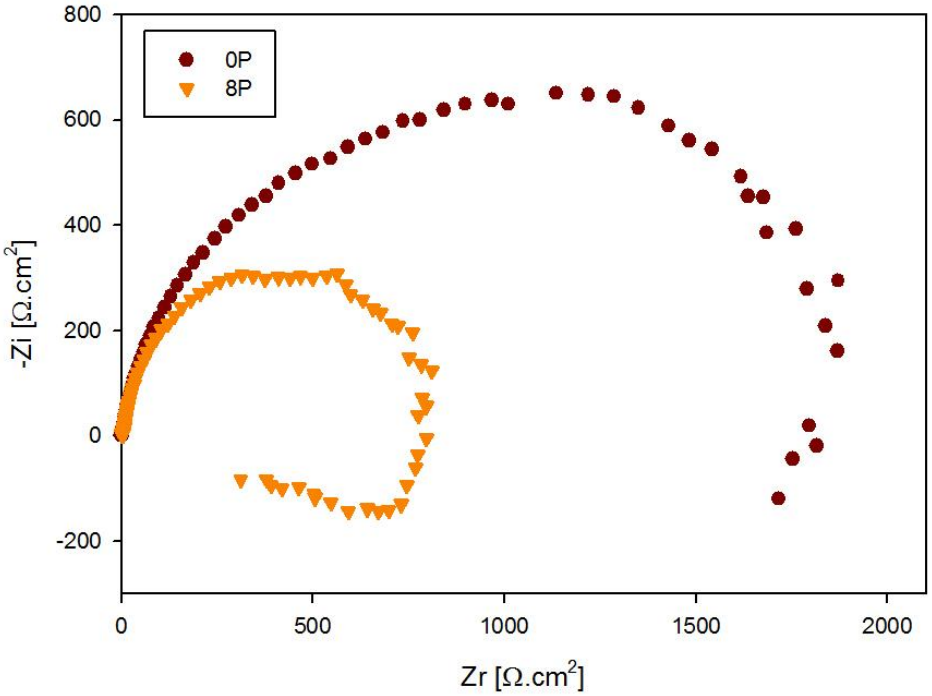

Figure 19: EIS characteristics of AE42 alloy, as extruded and ECAPed, in the solution with the pH of 12

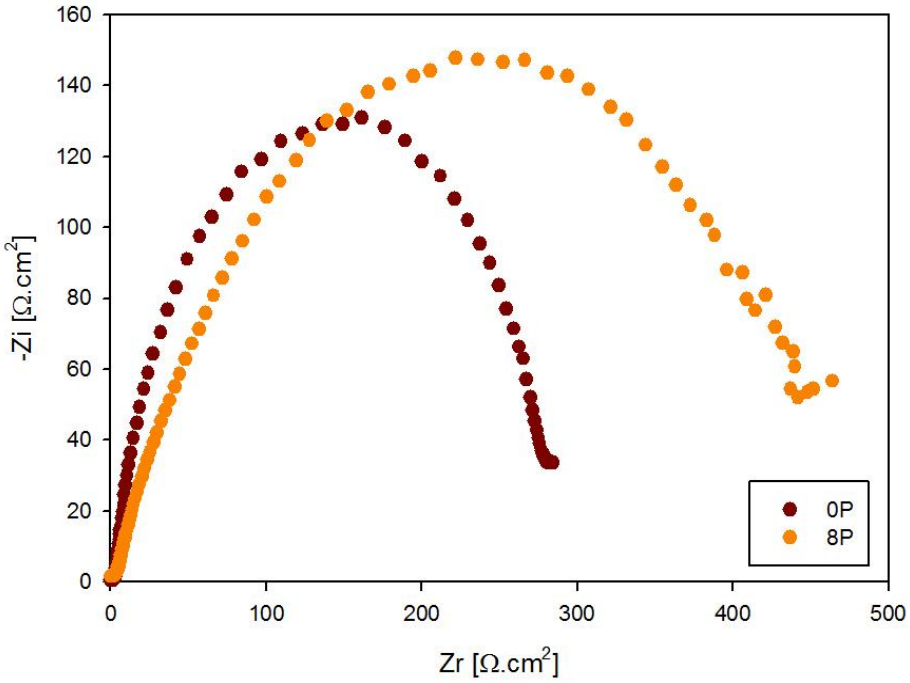

Figure 20: EIS characteristics of AE42 alloy, as extruded and ECAPed, after 168 hours immersion time in the solution with the pH of 7.

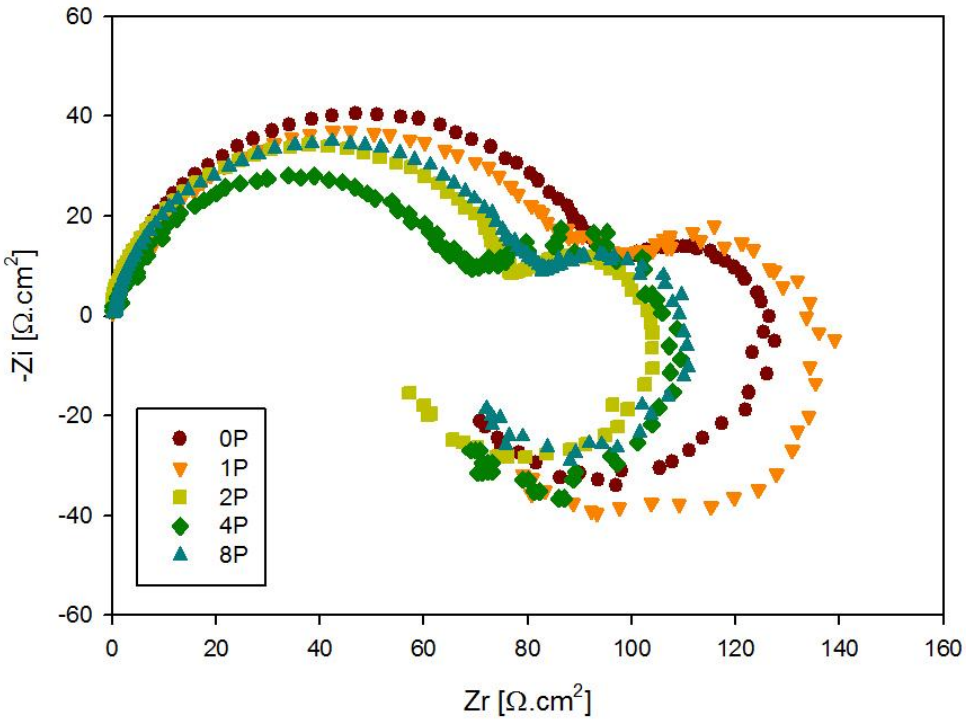

Figure 21: EIS characteristics of AE21 alloy with various number of ECAP passes in the solution with the pH of 7

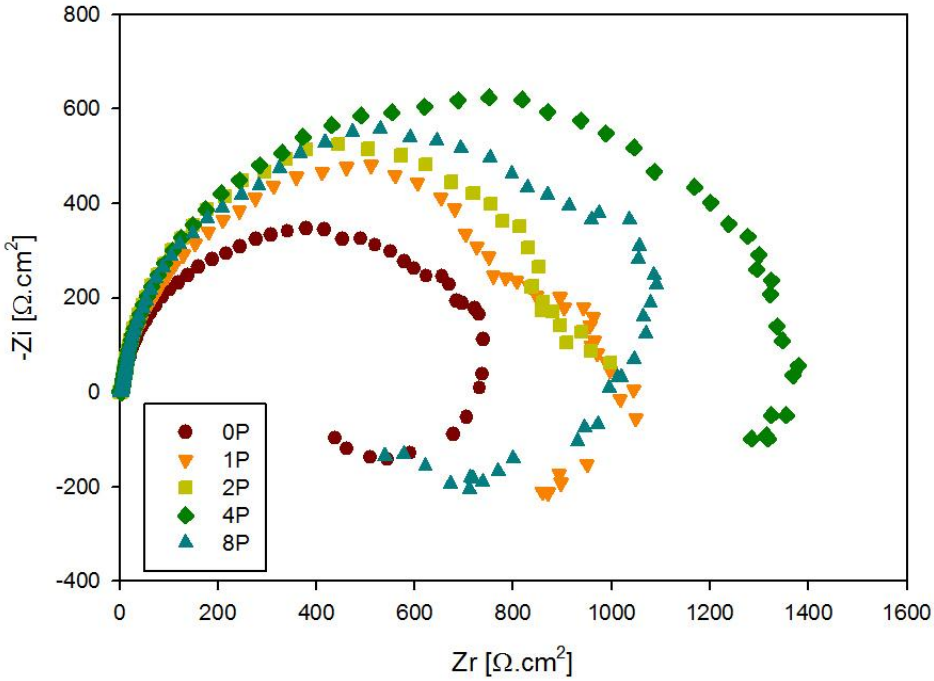

Figure 22: EIS characteristics of AE21 alloy with various number of ECAP passes in the solution with the pH of 12

For the characteristics measured in solutions with the pH of 7 three semicircles are typical, two in positive values of *-Zi*, one in negative values. Equivalent circuit of such dependence can be considered as the one presented on Figure 23 [55]. Equivalent circuit of dependence characterized by one semicircle, as are the most of characteristics measured in the pH of 12, can be considered as the one presented on Figure 24. Some characteristics measured in solution with the pH of 12 contain two semicircles, one positive and one negative and equivalent circuit of such dependence is presented as Figure 25 [7]. In all equivalent circuits are present parameters *Q*, which stand for constant phase elements. Total value of polarisation resistance is defined by the sum of resistance R_{p1}, R_{p2} (positive values of *-Zi*) and $-R_{p3}$ (negative values of *-Zi*), which are equal to diameters of the semicircles on the measured characteristics. In Table 5 and 6 are presented average values of measured R_p, obtained by equivalent circuit approximation.

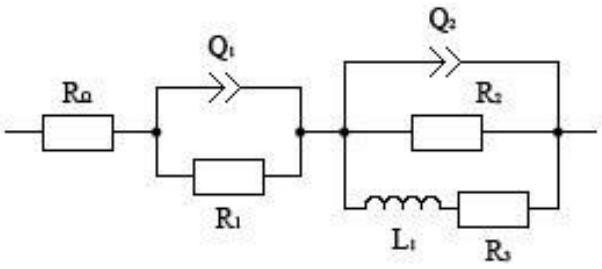

Figure 23: Equivalent circuit 1

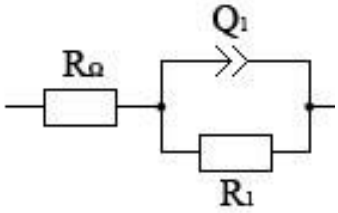

Figure 24: Equivalent circuit 2

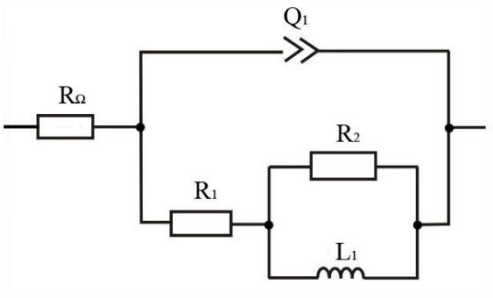

Figure 25: Equivalent circuit 3

Table 5: Average values of R_p [Ω.cm^2] of AE42 alloy

	pH 7	pH 12	168 hours
0P	120 ± 12	2194 ± 127	297 ± 44
8P	221 ± 22	432 ± 34	587 ± 70

Table 6: Average values of R_p [Ω.cm^2] of AE21 alloy

	pH 7	pH 12
0P	135 ± 13	396 ± 90
1P	117 ± 11	1085 ± 66
2P	105 ± 10	1041 ± 55
4P	104 ± 17	1285 ± 63
8P	103 ± 11	472 ± 82

From Tables 5, 6 and in corresponding/respective Figures is apparent that AE21 alloy, in solution with the pH of 7, loses its corrosion resistance with higher number of ECAP passes. Specimens with more than 2 ECAP passes had values of R_p approximately identical. AE42 alloy compared to AE21 alloy, gained almost double corrosion resistance after 8 ECAP passes than as extruded. The ECAPed specimen of AE42 alloy, after 168 hours of OCP stabilization, was also substantially more corrosion resistant than the as extruded specimen. In the solutions with the pH of 12 the results were different. Without an immersion prior to measurement, the AE42-8P specimen was significantly more corrosion resistant than AE42-8P, whereas after 168 hours immersion, the situation was just opposite. High differences are also between the AE21 specimens. To this contributed the induction semicircle measured in some specimens, which decreases the value of the corrosion resistance. Indications of the induction loop are able to find also in other characteristics, but are not such massive as in AE42-0P, AE21-0P and AE21-8P. Generally, specimens had higher corrosion resistance in solutions with higher values of the pH.

3.5 Immersion corrosion tests

Corrosion resistance of AE21 and AE42 alloys, as extruded and with eight ECAP passes, were investigated by immersion tests in the solution of 1% NaCl. Specimens were cut from the middle area of ECAPed billets due to numerous cracks found on the surface. The size of the specimens was 5 mm x 5 mm x 2 mm. Afterwards they were polished by 1200 emery paper. Values of the weight difference between initial and immersed specimens are presented in Table 7. The specimens were dried before the weight measurements. Uncertainty of measurement was estimated to be 0.02%. After 18 hours of immersion was noticed weight growth of the specimens because of expansion of the corrosion layer on the surface. After 143 hours was observed decrease of weight on non-ECAPed specimens, because of degradation of the surface layer. The layer was still growing on ECAPed ones. From values measured after 190 hours of immersion was deduced, that AE42 alloy with 8 ECAP passes is the most corrosion resistant from measured specimens. After next three days AE21-0P specimen disintegrated completely, AE21-8P approximately from 70%, AE42-0P less than 5% and AE42-8P were unchanged, what confirmed previous assumption. From this point was next investigation aimed mostly on AE42 alloy because of its enhanced corrosion resistance after 8 ECAP passes.

Table 7: Values of the weight difference [%] of AE21 and AE42 alloys immersed in 1% NaCl solution, errors are ± 0.02% in all cases

hours	AE21 0P	AE21 8P	AE42 0P	AE42 8P
18	+ 0.55	+ 0.43	+ 0.19	+ 0.05
143	- 14.32	+ 0.44	- 2.27	+ 0.23
190	- 61.34	- 7.63	- 2.70	+ 0.21

After finishing immersion test in 1% NaCl solution was AE42-8P specimen dried and immersed in Hank's balanced salt solution, without calcium & magnesium, with phenol red. Composition of Hank's solution presents Table 8. Final solution had the pH of 7.2 ± 0.2 and the osmolality of 271 ± 15, according to producer.

Table 8: composition [g/l] of Hank's balanced salt solution

KCl	KH_2PO_4	NaCl	Na_2HPO_4	$NaHCO_3$	D – Glucose
0.40	0.06	8.00	0.0477	0.35	1.00

In this solution was the specimen immersed for 36 days. First 6 days was placed in 50 ml container, exchanging solution every day, then in 500 ml container. In the end of the immersion time the specimen suffered 8% weight loss relatively to the value before the test, a 6.6% during the last 30 days of immersion

To exclude the possibility of influencing the measurement in Hank's balanced salt solution by the previous measurement in 1% NaCl, two other specimens were later prepared for the immersion test solely in Hank's solution. AE42-0P and AE42-8P specimens were prepared as is described above and placed for 30 days in the solution. After the time was up were both dried and softly cleaned. The weight differences between initial and immersed specimens were 2.4% for AE42-8P and 2.9% for AE42-0P. Unfortunately specimens did not have equal dimensions. 8P specimen had the plane perpendicular to the ECAP flow direction 1 mm wider. Also for additional observation by microscopes was the corrosion layer not completely removed. This two factors affected comparison of the weight difference of the specimens, nevertheless the data proved the higher corrosion resistance of the AE42 processed by ECAP.

3.6 Cytotoxicity of AE42 alloy

Cytotoxicity measurement provided information how much are studied specimens toxic to human body. Cytotoxicity was studied in vitro on the cell lines. There were used THP-1 human monocytes (human monocytic leukemia cells, ECACC 88087201), which were maintained in RPMI 1640 medium containing 10% fetal bovine serum, 2 mM glutamine and 1% penicillin/streptomycin (PAA Laboratories) at 37°C, 5% CO2. Before experiments THP-1 monocytes were seeded into 12-well plates at a density approximately $5x10^5$/ml.

Measurement was performed by determination of a cell viability using the trypan blue dye exclusion method (Vi-CELL, Cell Viability Analyzer, Beckham Coulter). In Figure 26 is shown initial condition of experiment. In Figures 27 and 28 are presented results after 23.5 hours exposure to AE42-0P and AE42-8P specimens. Comparing the viability of initial and after 23.5 hours exposure condition can be said, that AE42-8P specimen was double less toxic to cells than the as extruded specimen. Since the composition was the same, the difference can be attributed to lower corrosion rate of the AE42 processed by ECAP.

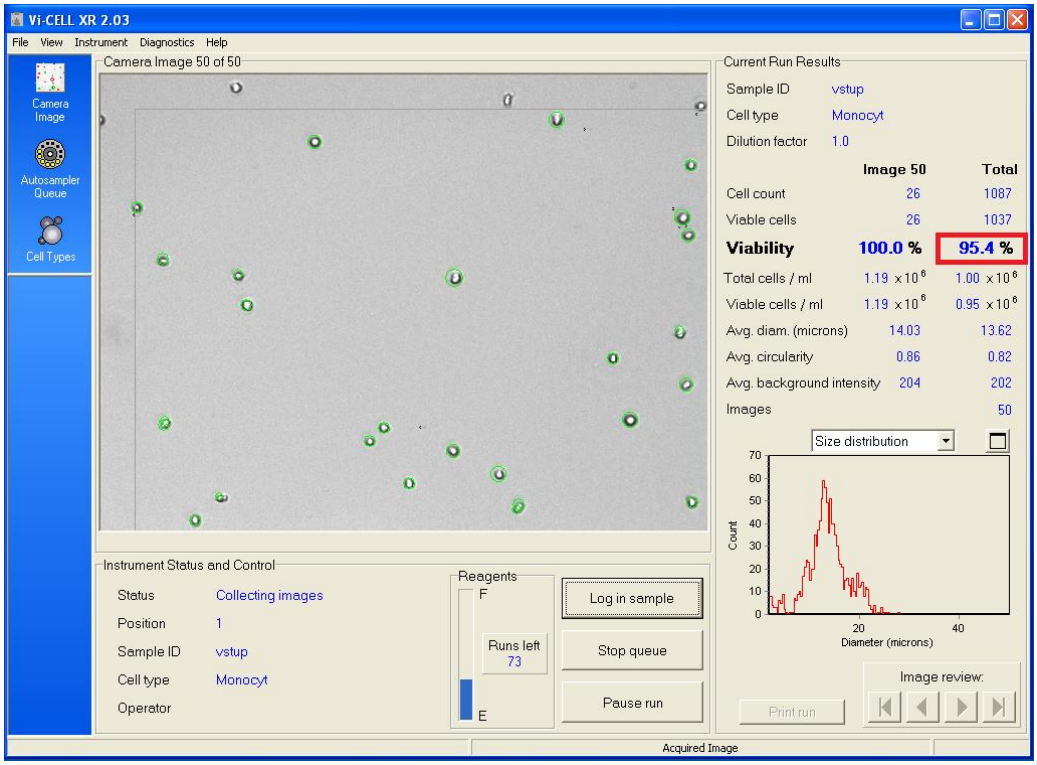

Figure 26: Initial conditions of experiment

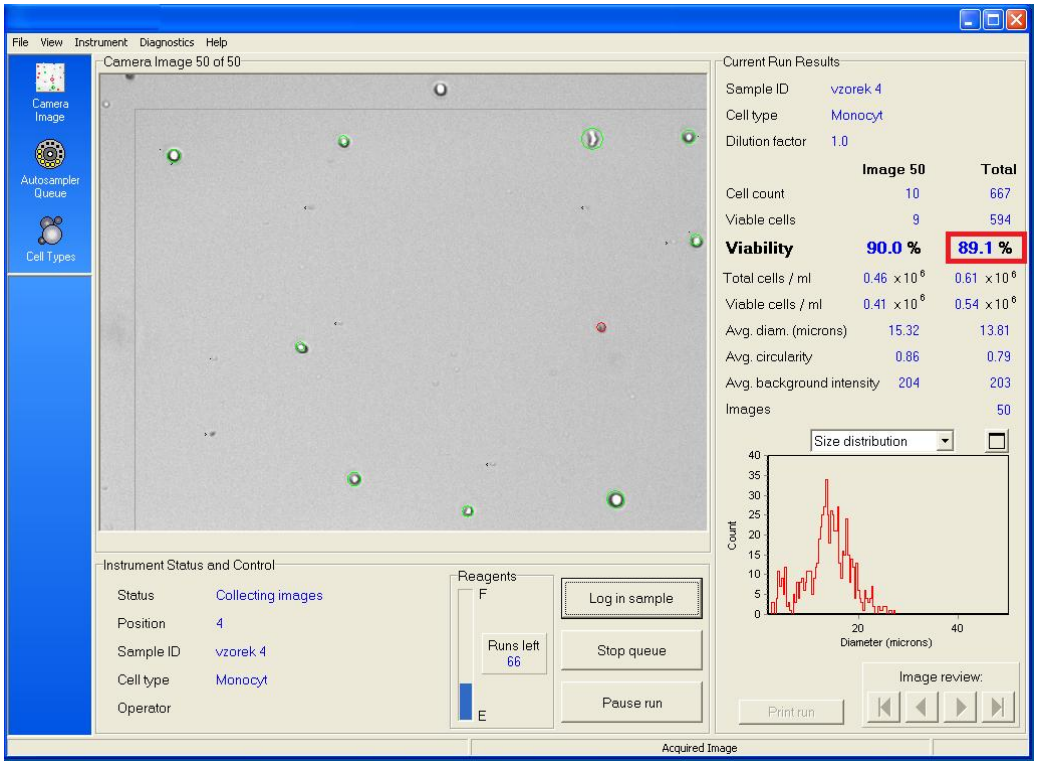

Figure 27: Cell viability after 23.5 hours exposure to AE42-0P

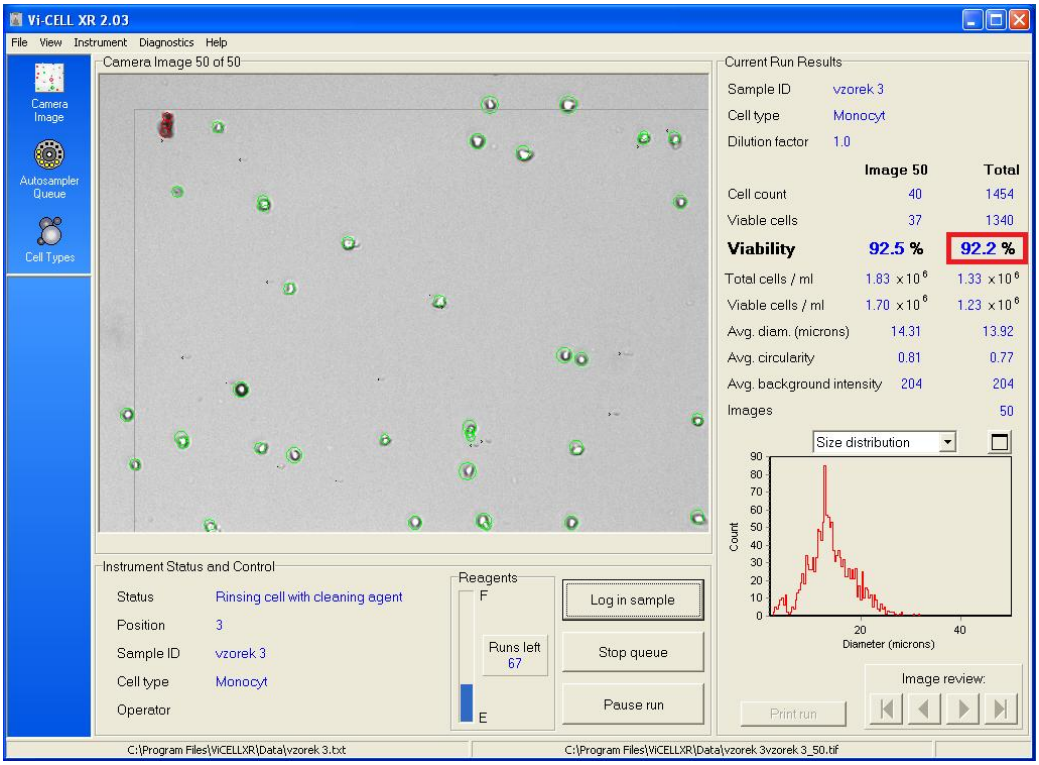

Figure 28: Cell viability after 23.5 hours exposure to AE42-8P

3.7 Examination of the corrosion layer and microstructure of AE42 alloy

Corrosion layer and microstructure of AE42-8P and AE42-0P specimens were investigated by SEM and metallographic microscopy. Following specimens were studied: AE42-8P after 11 days immersion in 1% salt solution and posterior 36 days immersion in Hank's solution and also specimen immersed for 30 days solely in Hank's solution. Both specimens had the same microstructure of the corrosion layer. AE42-0P specimen was immersed for 30 days in Hank's solution.

Specimens were mold into the epoxy resin prior to the observation and mechanically grinded to obtain observable cross section. Then the specimens were polished by 1200 and 2400 emery paper for two minutes both. Afterwards were polished by 3 μm polishing disc for three minutes. During polishing was added corresponding polishing paste and solution of 10% glycerine in alcohol.

Prior to the optical microscope observation, the specimens were also chemically polished by 1 μm polishing disc and OPS suspension. Afterwards were etched in picric acid for the time presented by each figure. On Figures 29-34 are presented metallographic photos of the cross section plane parallel to the ECAP flow direction.

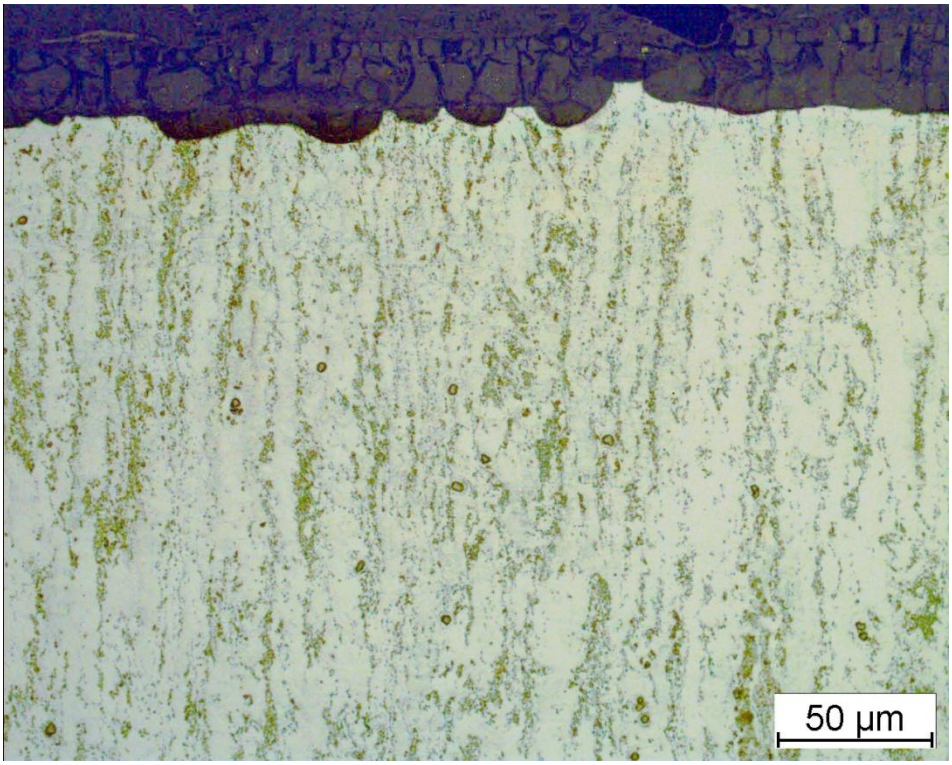

Figure 29: Cross section of AE42-8P specimen with corrosion layer, etched for 5 seconds

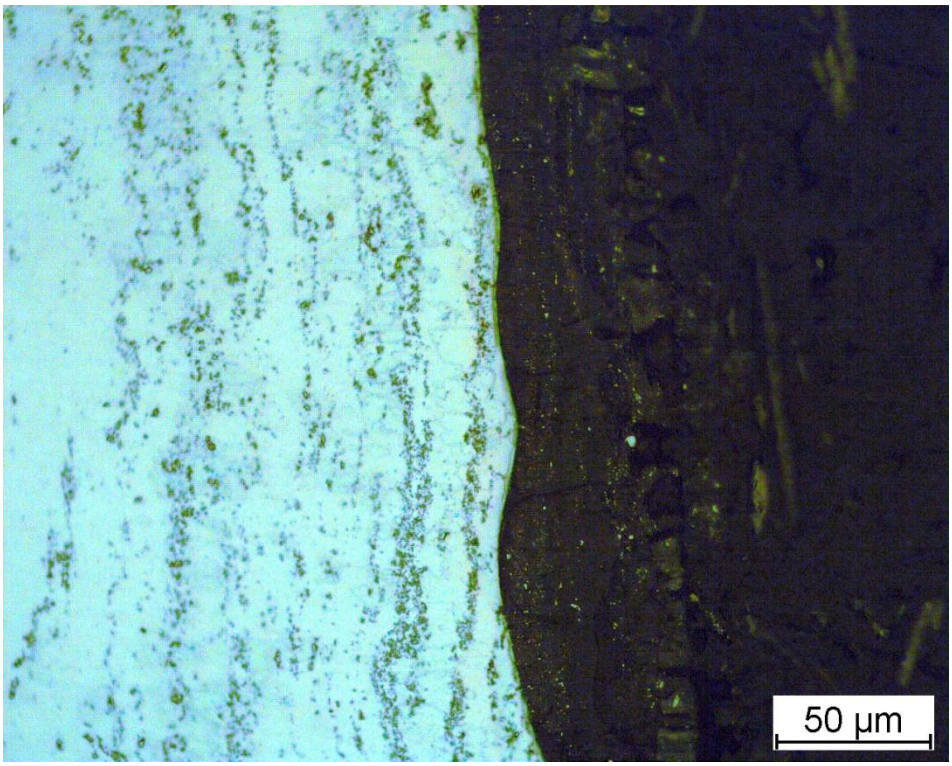

Figure 30: Cross section of AE42-8P with corrosion layer, etched for 5 seconds

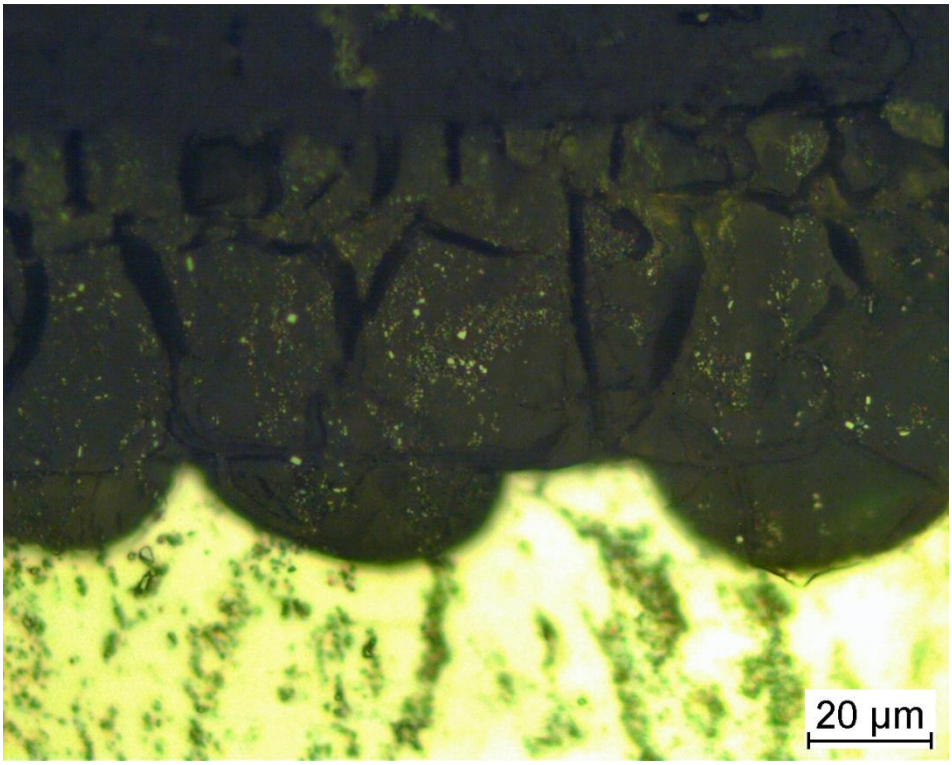

Figure 31: Detail of the corrosion layer of AE42-8P specimen, etched for 5 seconds

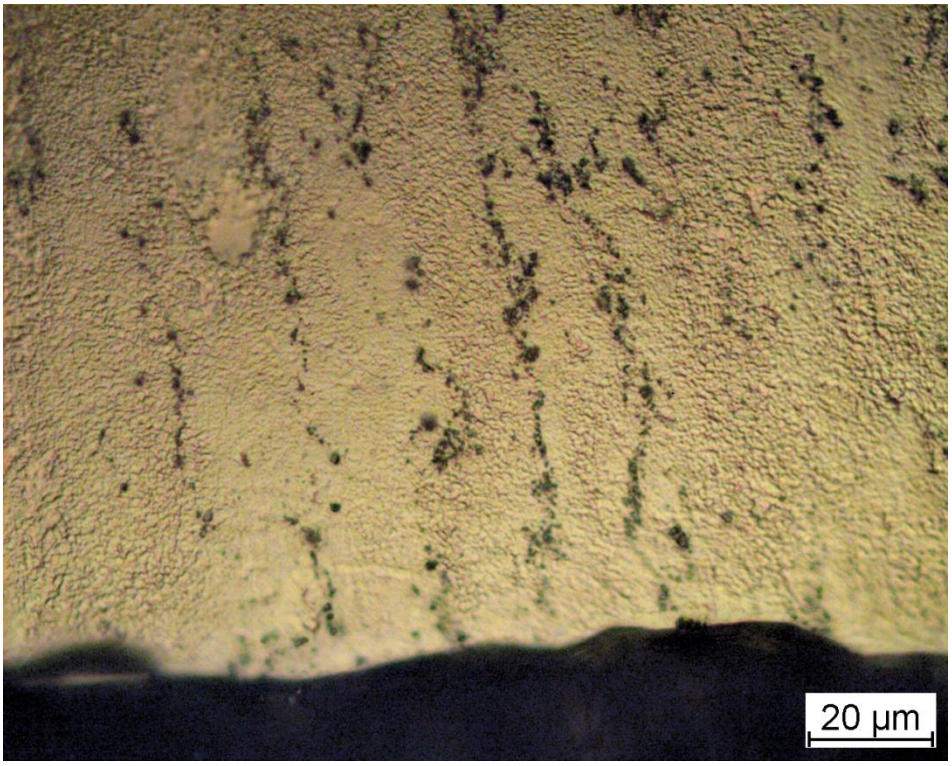

Figure 32: Detail of the microstructure of AE42-8P specimen, etched for 40 seconds

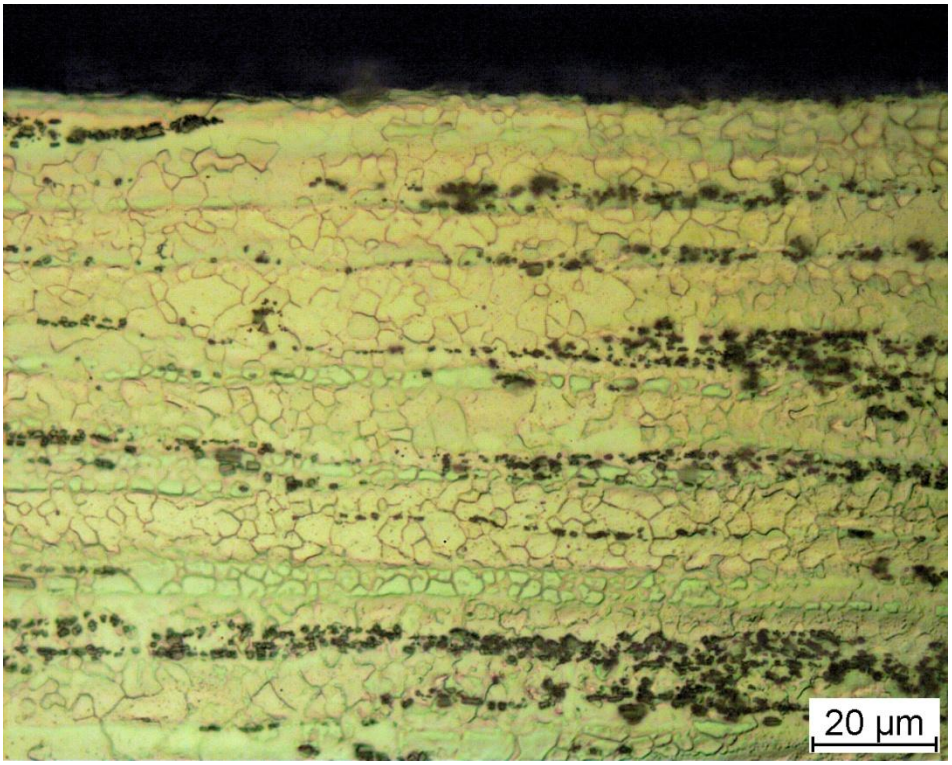

Figure 33: Detail of the microstructure of AE42-0P specimen, etched for 15 seconds

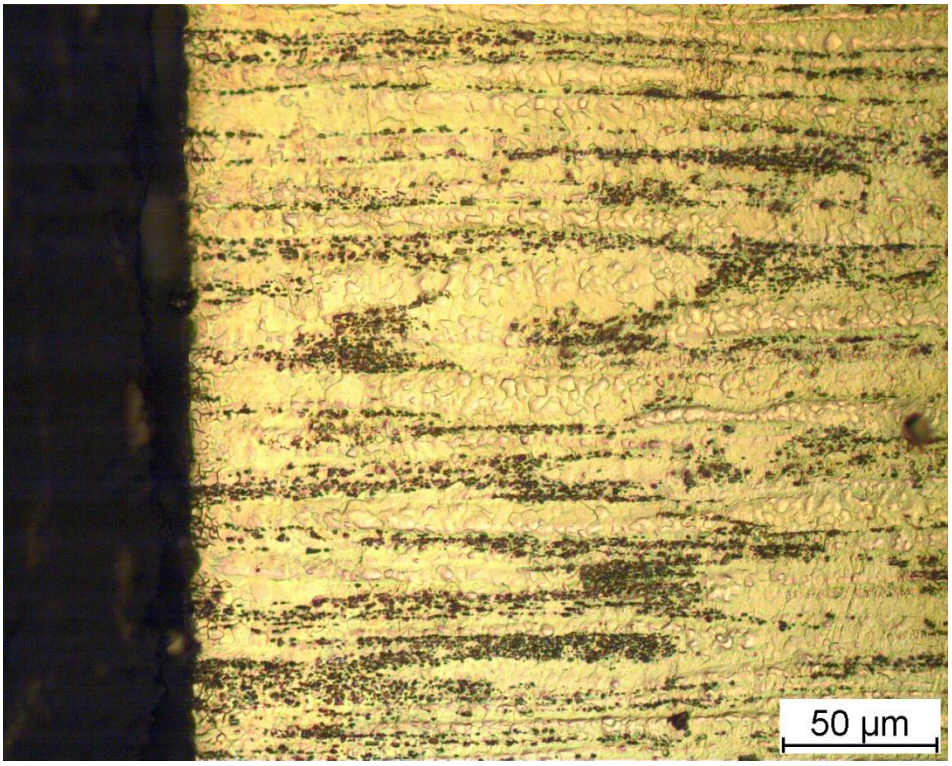

Figure 34: Microstructure of AE42-0P specimen, etched for 15 seconds

On Figure 29 and Figure 30 there are observed stripes generated by dispersed particles in the direction of the ECAP pressing. The corrosion layer created on the edge of the specimen is different depending on the angle between the layer and the stripes. The layer perpendicular to the stripes direction is much more disordered, full of cracks and cavities, and the boundary between untouched metal and the corrosion layer is rougher than the boundary parallel to the stripes. Detail of the corrosion layer perpendicular to the stripes is presented as Figure 31. Bright dots in the corrosion layer are apparently dispersed particles according to continuous crossing of the stripes through the boundary. Figures 32 and 33 are presented as comparison of the microstructure of the as extruded specimen and the ECAPed specimen. The grain refinement after ECAP pressing is obvious. Figure 34 shows distribution of the dispersed particles in the as extruded specimen. Stripes structure of the dispersed particles was also observed, but in the as extruded specimen were the particles much more concentrated.

More detail photos of the boundary between the corrosion layer and of the untouched metal were taken by SEM. Chemical analysis of dispersed particles was performed by EDS. Prior to the SEM observation the specimens were polished by 3 μm and 1 μm polishing disc for three and four minutes, respectively. During polishing was added corresponding polishing paste and solution of 10% glycerine in alcohol.

For the 8P specimen is a complex overview of the specimen's edge shown on Figure 35. On Figure 36 and Figure 37 is presented closer view on the corrosion layer and non-corroded area beneath it. On Figure 36 is the layer perpendicular to the stripes and on Figure 37 parallel. On Figure 38-41 are shown details of corrosion layers of the as extruded specimen. The angle between the layer and the stripes is apparent from each Figure.

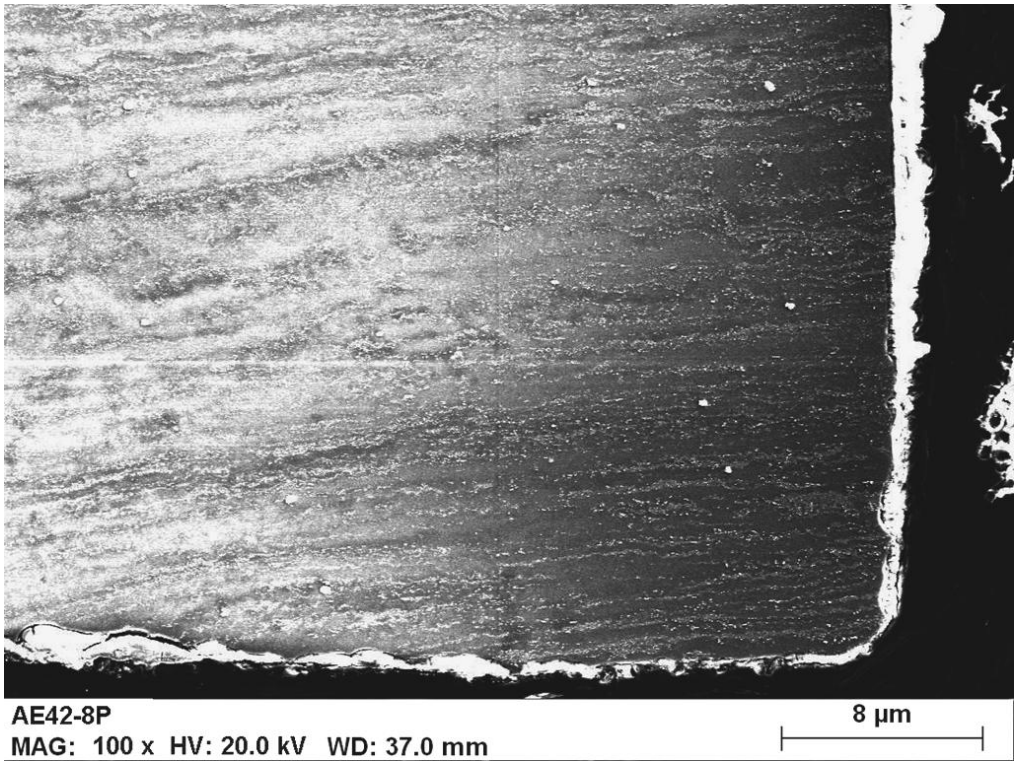

Figure 35: Edge overview of the AE42-8P specimen

Figure 36: Corrosion layer of the AE42-8P specimen

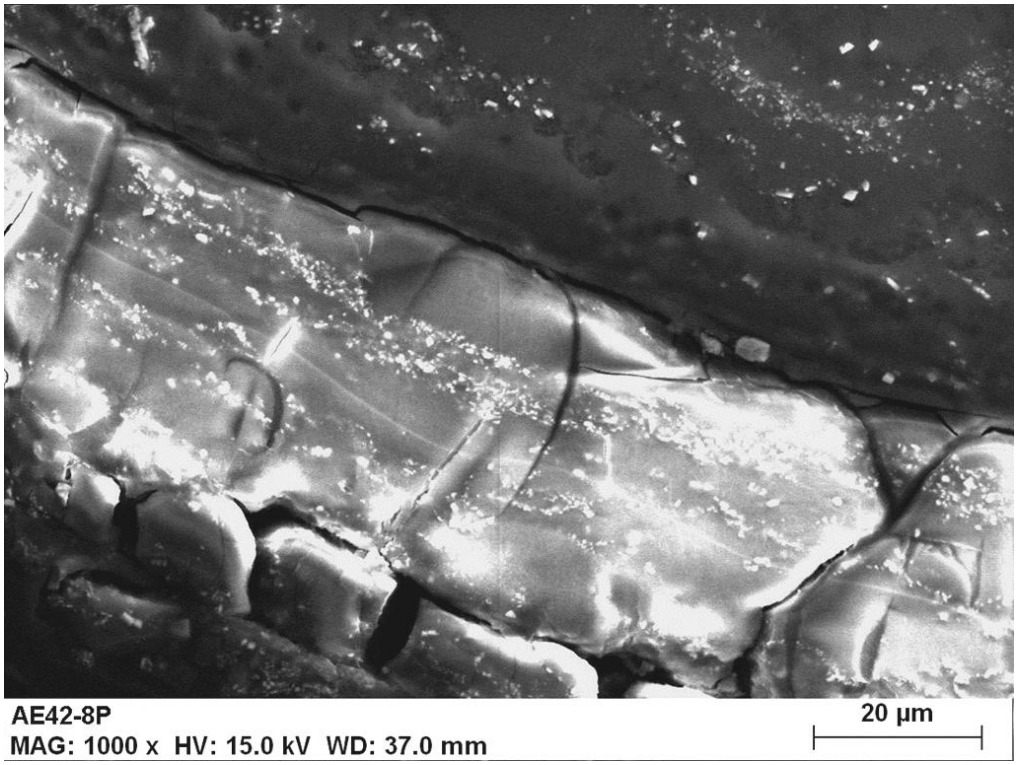

Figure 37: Corrosion layer of the AE42-8P specimen

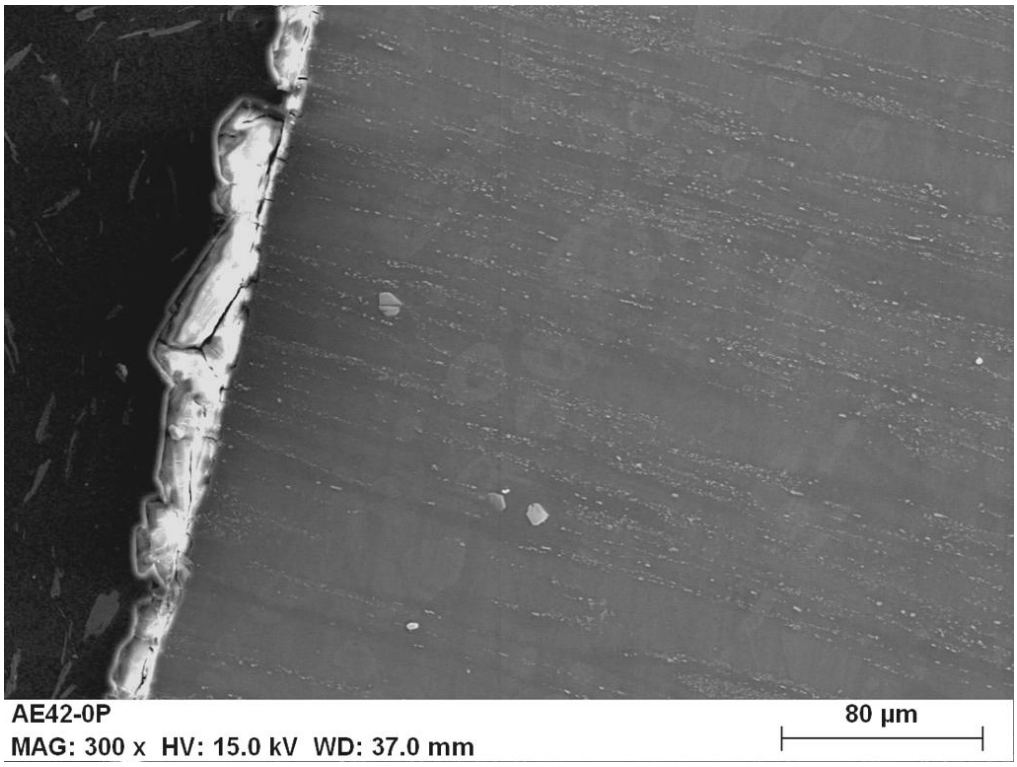

Figure 38: Corrosion layer of the AE42-0P specimen

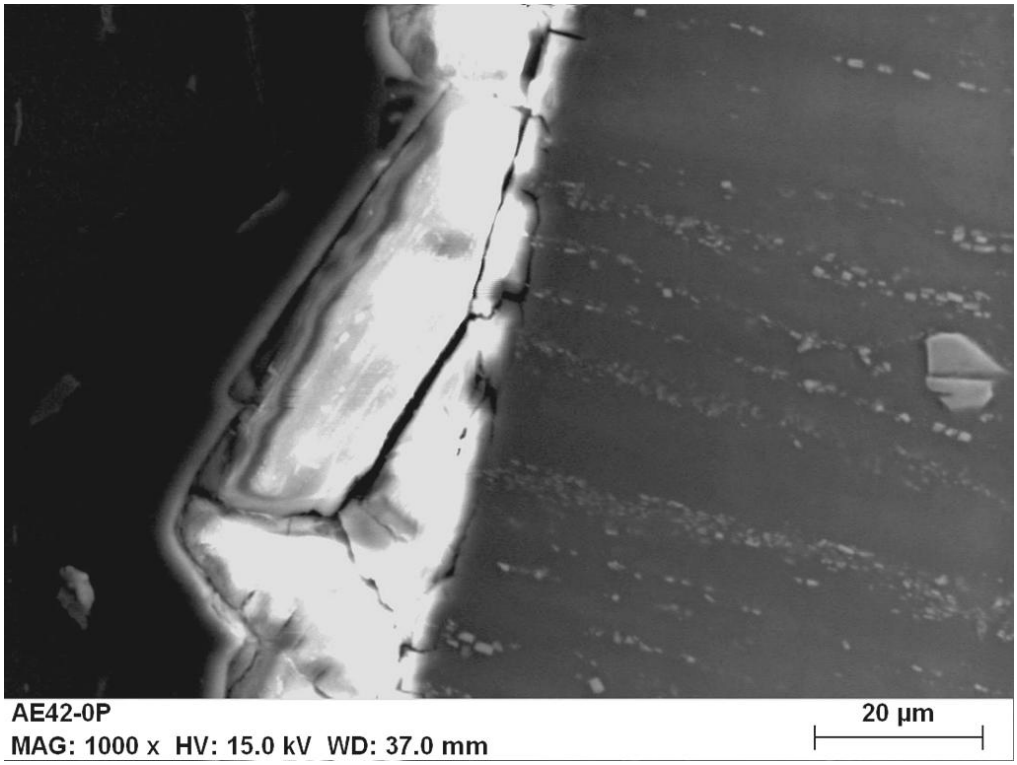

Figure 39: Corrosion layer of the AE42-0P specimen

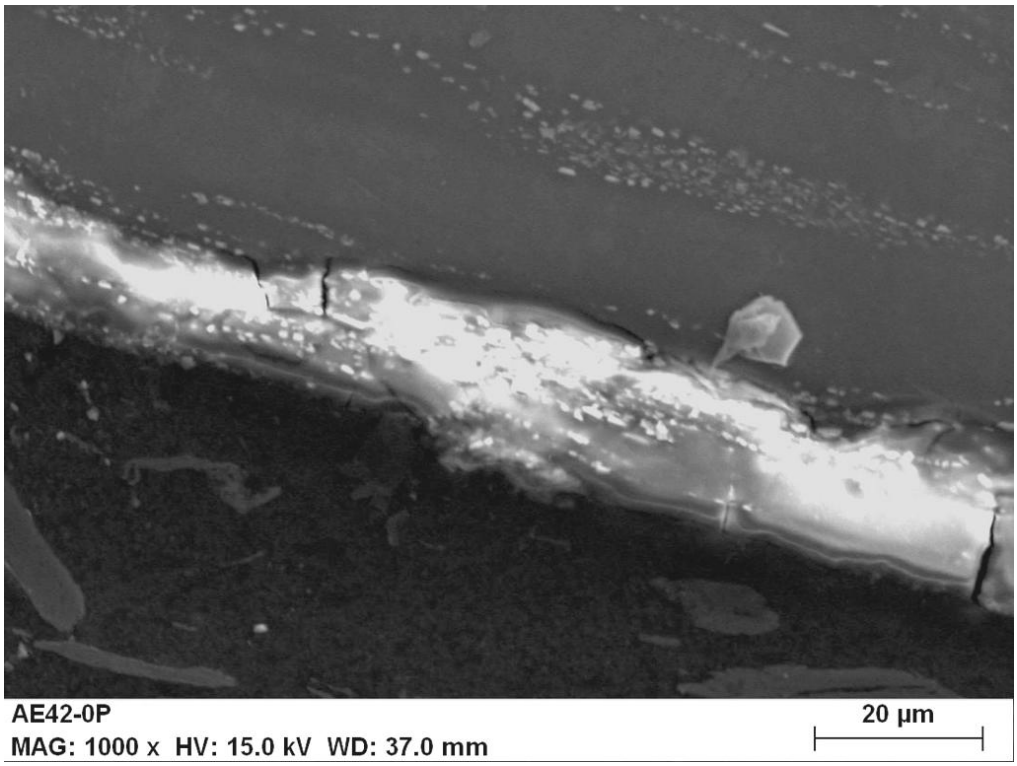

Figure 40: Corrosion layer of the AE42-0P specimen

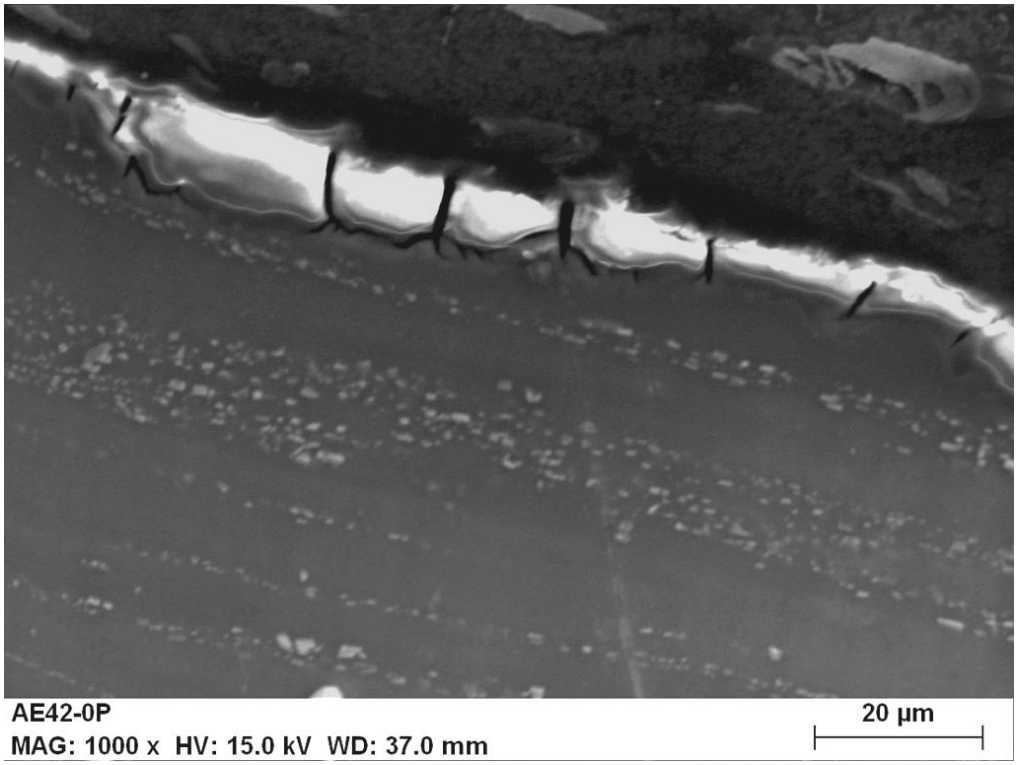

Figure 41: Corrosion layer of the AE42-0P specimen

On Figure 35 is the corrosion layer displayed as the bright stripe around the metallic specimen due to hypercharge of the layer. On majority of previous Figures there are present particles of higher diameter than the mentioned dispersed ones and the same particles can be found also scattered on Figure m1. They were identified by EDS analysis as $MnAl_4$. Particular diffractogram is presented as Figure 43.

By comparison of Figure 36 and 38 or Figure 37 and 40 can be said, that the corrosion layer of the specimen after 8P was substantially thicker than the layer of the as extruded specimen. On Figure 39 is shown detail of the corrosion layer of the as extruded specimen. The size of the area that is about to separate from specimen's surface is much larger, than parts of the corrosion layer that are about to separate from the surface of the ECAPed specimen, as shown on Figure 36.

Dependence of stability of the corrosion layer on the angle between the layer and the stripes, created by dispersed particles, was studied by light microscope. It was shown that the stripes parallel to the corrosion layer enhanced corrosion resistance. On Figure 40 is presented the layer rich on dispersed particles that is without larger cracks and cavities and is approximately two times wider, than the layer almost without dispersed particles (Figure 41), where large cracks are found.

Figure 42 shows composition of the area around the corrosion layer and metal boundary observed by EDS. From this figure can be concluded that dispersed particles generating the stripes are composed from aluminium and rare earth elements. EDS analysis of the single particle

was performed three times with result that composition is within the error $Al_{11}RE_3$ and one of the diffractograms is presented as Figure 44.

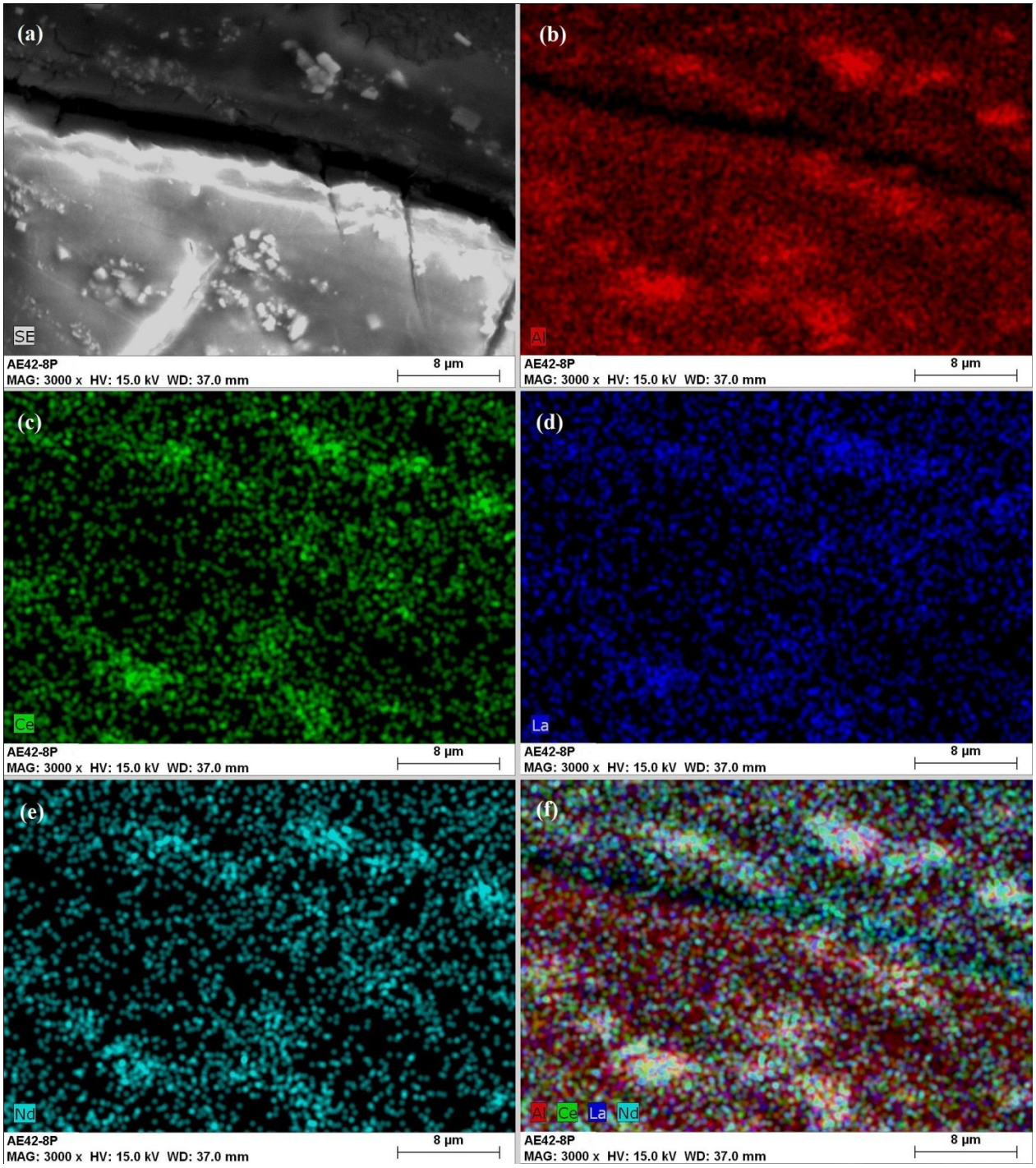

Figure 42: Composition of the area around the corrosion layer – metal boundary of the AE42-8P specimen: (a) overview, (b) aluminium, (c) cerium, (d) lanthanum, (e) neodymium, (f) aluminium with rare earth

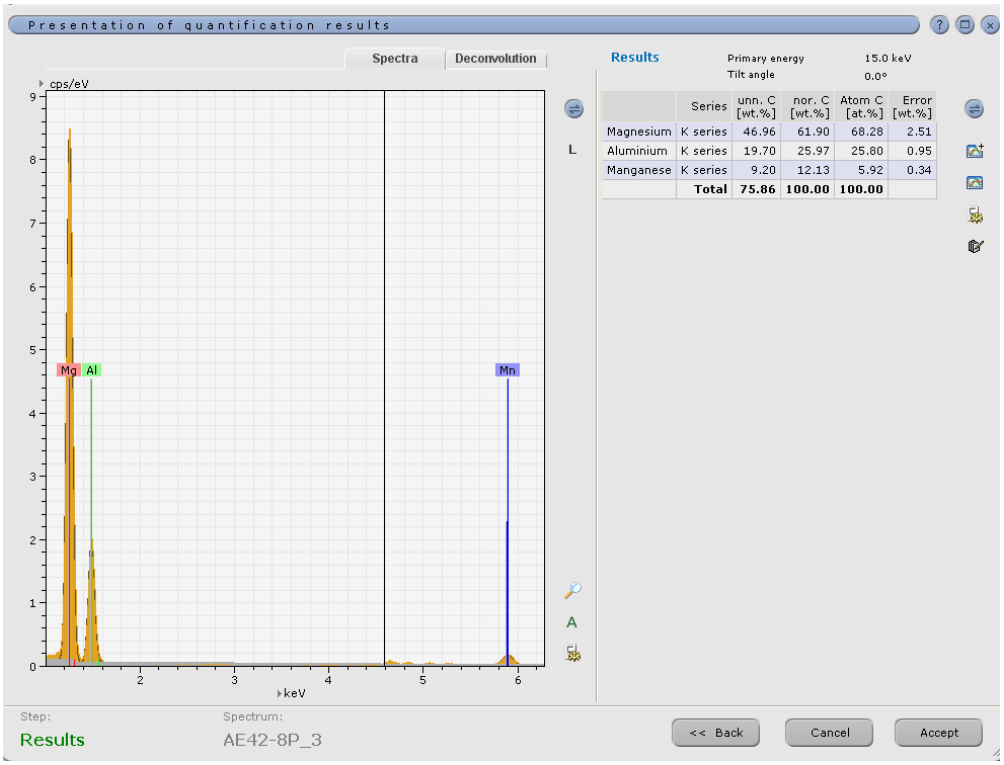

Figure 43: Diffractogram of the particle of higher diameter in the AE42-8P specimen

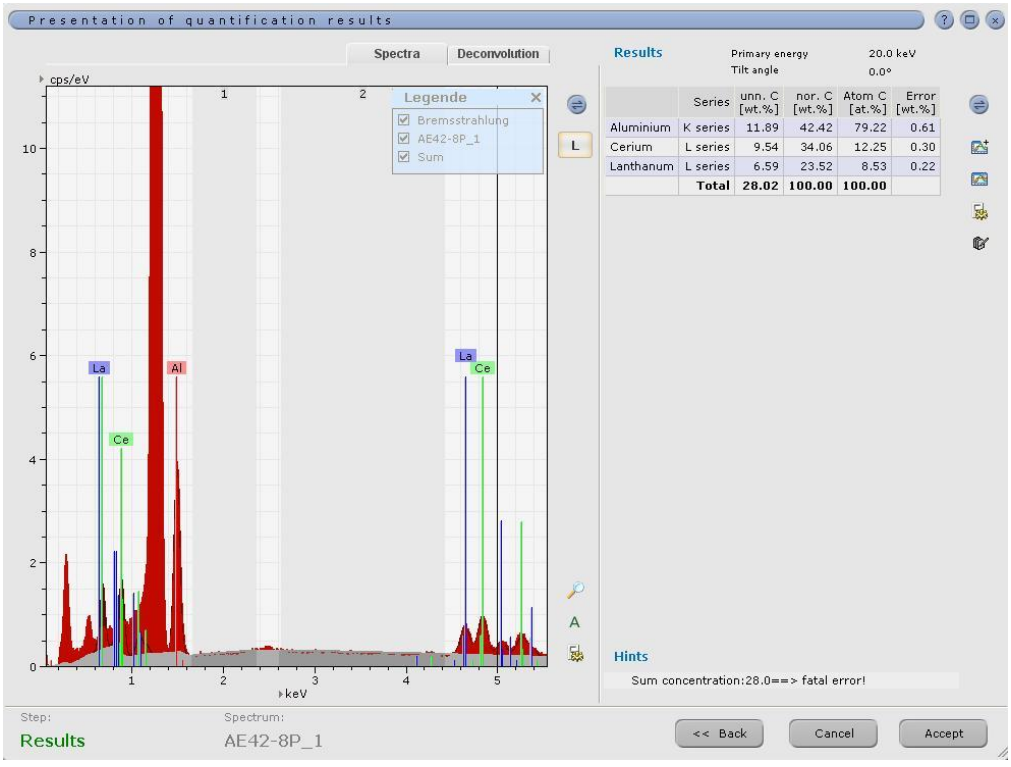

Figure 44: Diffractogram of one of the dispersed particles in the AE42-8P specimen

3.8 Thermal stability of dispersed particles in AE42 alloy

Stability of the dispersed particles was observed by DSC. The as extruded specimen of AE42 alloy was cut from the inner part of the billet, as specimens designated for the immersion tests. The specimen was then polished by 1200 emery paper and degreased. Weight of the specimen was 13.3 mg. The measurement was performed within the limits of 80-500°C with heating rate 10°C/min. Resultant plot is presented as Figure 45. Inhomogeneous starting area of the experiment was cut-off. From this Figure is apparent, that all components of AE42 alloy were stable till 500°C.

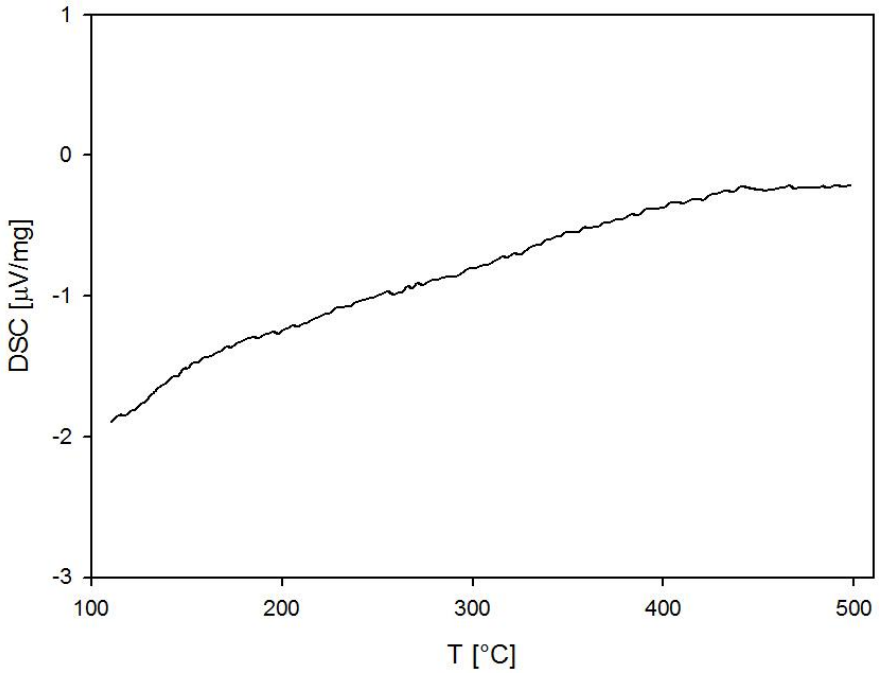

Figure 45: DSC characteristic of AE42 specimen

4 Discussion

Mechanical and corrosion properties of AE21 and AE42 alloy with different number of ECAP passes were investigated. The grain refinement after ECAP treatment should lead to elevation of the yield stress as is given by the Hall – Petch equation, but after two passes the yield strength started to decrease. The difference between the grain size of the as extruded and 8P specimen is apparent from the comparison of Figure 33 and 34. It was noted that the yield strength decreases after grain refinement under approximately 100 nm, because of the inverse Hall – Petch relation [44]. But as was shown by TEM observation, after eight passes the microstructure was still bimodal with larger grains 2-3 μm of the diameter. The answer is most likely that the softening appeared because of changes in texture and dislocation densities between each ECAP pass, as presented in [49].

The grain refinement also improved possibilities for superplastic treatment as shown on Figures 10 and 11. AE21 alloy gained localized massive elevation of the *m* parameter in strain rates near $3x10^{-4}$ s^{-1}. AE42 alloy had the highest values also near the same strain rate, but after 8P the specimen exhibited a higher *m* parameter on the whole measured interval. Examination of the superplasticity was conducted namely to assess the effect of secondary phase particles on stabilization of microstructure since the particles play an important role in corrosion process, too. An additional study would be needed in order to find the best parameters for the superplastic process. Effect of grain refinement to enhance *m* parameter is noted in numerous works. For example in [56] was achieved 1320% elongation in AZ61 alloy using Ex-ECAP method. In [57] was studied effect of Ex-ECAP method on AZ31 and between temperatures 350-450°C with strain rates up to 10^{-4} s^{-1} were achieved elongations up to 1000% with *m* parameter approximately 0.5.

Corrosion is a process that occurs primarily at the surface defects, such as grain boundaries and dislocations. When the specimens were put in the solutions, the corrosion process immediately began preferring these sites. The ECAPed specimens had substantially more nucleation sites for the formation of an oxide or a passive film than the as extruded specimens. Magnesium dissolution in aqueous environment creates partially passive film $Mg(OH)_2$ and H_2 in gaseous form. Stability of the film depends on the pH of the solution. In the solution with the pH of 11 and higher is the film stable [58], and therefore the specimens studied in the solution with the pH of 12 had higher values of polarisation resistance, than specimens studied in the same solution with the pH of 7, as presented in Table 5 and 6 . In case of the high difference between i_{cor} values of the as extruded specimen and the ECAPed specimens of AE21 alloy (see Table 4), it can be ascribed to the more rapid creation of the passive film on ECAPed specimens, due to higher number of nucleation sites, and therefore suppressed charge transfer [59]. Also there is a difference between ECAPed and non-ECAPed specimen of AE42 alloy, where the same reason is considered. In some PD characteristics measured in the pH of 12 (Figure 16 and 17), the applied current rapidly increased once the potential reached a sufficiently positive value. This increase was assumed to appear because of localized breakdown of passivity (pitting) [50]. The E_{cor} values

are shifted to more noble ones than values measured in the pH of 7, what also corresponds to creation of the stable passive film.

The character of the Nyquist plot can be quite different depending on the type of physical process acting on the solution – metal interface. In case of semicircles, as were measured for all specimens in the solutions, capacitive loop ($-Zi > 0$) represent charge transfer resistance and double layer capacitance and inductive loop ($-Zi < 0$) is related to the relaxation of adsorbed products [7] and/or activation of the corrosion microcells close to the interface. These microcells can occur between microstructures of different nobility or between the metal and nobler corrosion layer [55]. This particular character had the measured data of specimens studied in the solutions with the pH of 12. In case of the pH of 7 the characteristics had two capacitive semicircles. There are two ways to explain this phenomenon. The first is that on the interface are present two layers, one porous and one non-porous – isolative, and the loops represent the layers individually [55]. The second is that the first loop represents the only layer on the interface that is partially coating the metal and the second loop represents points, where this coating layer is failing and new interface is made by a pocket filed with an electrolyte solution different from the rest [52]. According to the examination of the corrosion layer by light microscopy both mentioned scenarios were involved in the corrosion process. On the interface perpendicular to the stripes, which are created by dispersed $Al_{11}RE_3$ particles, dominated failing coating according to observed roughish interface and also according to areas of the semicircle shape where in the centre could have started the failing (see Figure 31). On the interface parallel to the stripes the layer was smoother and therefore the layer could be formed by outside porous and inner non-porous corrosion layer (see Figure 30). Nevertheless, also in some places on the interface parallel to the stripes semicircle areas were found.

When the pH is lower than 11 the film of $Mg(OH)_2$ is only partially protective. For that reason the polarisation resistance of specimens measured in the pH of 7 was significantly lower. The polarisation resistance of AE21 alloy specimens decrease after ECAP pressing and after two and more passes is equal in the limit of uncertainty, as presented in Table 6. Similar dependence of the R_p on the number of ECAP passes was presented in [59], where pure magnesium underwent examination. The polarisation resistance (in Figure 18) of the AE42 alloy specimen with eight ECAP passes was higher than as extruded one, almost double. In difference of AE21 alloy, AE42 alloy contains double weight percentage of aluminium and rare earths, which are assumed to slow down corrosion process. In order to examine long time corrosion resistance were the AE42, as extruded and ECAPed, specimens immersed in the 1% NaCl solution for 168 hours and afterwards EIS tests were performed and presented as Figure 20. It was confirmed, that AE42-8P specimen has higher corrosion resistance even after longer immersion time.

Disappearance of the second capacitive semicircle when the pH was higher can be explained by creation of the single non-porous passive film of $Mg(OH)_2$. As mentioned earlier, according to findings from PD tests, this protection film breaks after reaching a certain value of E_{cor} and pitting corrosion process takes place. Disappearance of the second capacitive loop after 168 hours exposure is ascribed to the unification of the processes that take place on the solution – metal interface. According to [55] the non-porous layer merged with the outside

porous. Vanishing of the induction loop after the long immersion time can be attributed to the reduction of the $Mg(OH)_2$ and /or MgO layer thickness [7].

Differences between values of E_{cor} are probably not significant, because in [60] was determined, that values of E_{cor} are able to shift in early stages of the corrosion process of magnesium alloys for up to 0.05 V. Saturated values of E_{cor} should be taken after 25-30 minutes of stabilization. For that reason the high differences in the results of EIS tests for AE21 and AE42 alloy (Table 5 and 6), in the solution with the pH of 12, are the most probably caused also by irregularity of the early stage creation of the corrosion layer.

Uncertainties of measured electrochemical characteristics are different and occasionally high. It is mainly because of non-homogeneity of the studied structure that affected the measurement and therefore each time after polishing was the surface different. Also local microcracks could be present what also put some difference between measurements. In the last place bubbles of oxygen were accumulating on the electrodes what affected true value of working area of the electrodes. To decrease the value of uncertainty a higher number of measurements would be necessary.

The immersion corrosion tests were conducted in such a way to be able to compare studied alloys, their treatments and preparation of the specimens to posterior observation by microscopes. In a standard test, corrosion layers should have been removed completely before the weight measurements and specimens should have had one dimension irrelevant compared to other two [51], but in this case it was important, that the difference between the AE21 and AE42 alloy after 11 days of immersion was significant, as is presented in Table 7. The weight difference between AE42 as extruded and AE42-8P was bigger in the first test performed in 1% NaCl solution, but also in the test performed in Hank's solution for 30 days the ECAPed specimen was more corrosion resistant. As was shown by metallographic microscopy, the corrosion layer is different depending on the angle between the layer and the stripes created by dispersed particles. Therefore differences in individual dimensions can affect the final mass loss. The AE42-8P specimen had the surface perpendicular to the stripes 25% (1 mm) wider, and for that reason the corrosion rate could be higher than in as extruded specimen, and therefore the difference could be bigger. Also the weight differences measured for AE42-8P specimen immersed in salt and Hank's solution and the specimen immersed only in Hank's solution was not a like, also because of different dimensions of the specimens. Also periodic drying of the specimen before weight measurement during the test in the salt and Hank's solution affected the final weight loss. Therefore these values cannot be easily compared to values from the literature. Nevertheless it can be concluded that the corrosion resistance was substantially higher than in magnesium Nd2 alloy that had weight loss 16% after 30 days of immersion in 0.9% NaCl solution [61]

The corrosion layer created on the surface was observed, and a difference between the layers created on the AE42 alloy specimen, as extruded and after 8P, was found. The main difference is the thickness of the layer. The ECAPed specimen had after 30 days of the immersion the layer substantially thicker than the as extruded specimen immersed for the same

time, as is apparent by comparison of Figure 36 and 38 or Figure 37 and 40. It was observed, that the layer of the as extruded specimen is separating by larger areas than of the ECAPed one (Figure 39), and therefore the protective layer decomposes more quickly. As was mentioned above, the microstructure of AE42 alloy was composed of $Al_{11}RE_3$ dispersed particles creating stripes. The difference between the layer created parallel to the stripes and the layer created perpendicular to them was found. Parallel stripes of $Al_{11}RE_3$ dispersed particles enhanced the corrosion resistance by slowing down the progress of the reaction, due to protection against separation of larger areas and inhibition of cracks propagation through the layer, as is apparent by comparison of Figure 40 and 41. The effect of the particles in the ECAPed specimen was higher, because the ECAP pressing made their distribution more uniform.

DSC measurements performed up to 500°C did not reveal any phase transformation in the AE42 as extruded specimen (Figure 45), which is in accordance with the fact that the $Al_{11}RE_3$ phase is stable up to temperatures above the melting point of the alloy.

5 Conclusions

Mechanical and corrosion properties of AE21 and AE42 alloys were investigated with respect to the number of ECAP passes. The yield strength of AE21 alloy was decreasing after two passes as was proposed in the literature. The grain refinement after ECAP pressing enhanced the superplastic behaviour of both alloys with the highest strain rate sensitivity index near $3x10^{-4}$ s^{-1} for both.

Immersion corrosion tests in 1% NaCl solution excluded the AE21 alloy for further investigation due to massive weight loss through the corrosion process. The AE42 alloy was much more corrosion resistant and the specimen after eight ECAP passes had the best results among all specimens. Also electrochemical corrosion tests confirmed its superior corrosion resistance in the solution of 0.1 M NaCl with the pH of 7 with OCP stabilization for five minutes and also for 168 hours. The dependence of the corrosion layer on the microstructure was observed in AE42 specimens. The microstructure contained stripes of $Al_{11}RE_3$ dispersed particles in the as extruded and also in 8P specimens. The corrosion layer created on the surface of the ECAPed specimens was different depending on the angle between the stripes and the layer. The dispersed particles enhanced corrosion resistance and stabilized the layer. Difference in the thickness of the created layer between the as extruded and the ECAPed specimen was found. The layer on the ECAPed specimen was compact and thicker than the layer created on as extruded one, where larger areas of the layer were separating from the surface.

AE42-8P specimen had superior results also in cytotoxicity measurements, the most probably due to higher corrosion resistance. DSC measurements performed up to 500°C did not reveal any phase transformations in the AE42 as extruded specimen, which is in accordance with the fact, that the $Al_{11}RE_3$ phase is stable up to temperatures above the melting point of the alloy.

It has been shown that the ECAP process can substantially increase corrosion resistance in magnesium-aluminium-rare-earth alloys with potential for biodegradable applications. However, these results still have to be confirmed in the experiments in vivo, since the in vitro test can bring antipodal results as it has been demonstrated in [62] where three different alloys were studied in vivo and the alloy which had the best results ended afterwards as the worst in the in vitro tests. Nevertheless, we can be rather optimistic as regards the in vivo behaviour since the ECAP process affect only microstructure, not the composition of the material, and a deterioration of the corrosion properties in vivo after the ECAP processing is thus very improbable.

6 References

[1] B. L. Mordike, T.Ebert: Mat. Sci. Eng. A 302 (2001), 37
[2] B. Heublein, R. Rohde, V. Kaese: Heart 89 (2003), 651.
[3] J. Nagels, M. Stokdijk, P. M. Rozing: J. Shoulder Elbow Surg. 12 (2003), 35.
[4] B. Heublein, R. Rohde, V. Kaese, M. Niemeyer, W. Hartung, A. Haverich: Heart 89 (2003), 651.
[5] A. Mussi, J. J. Blandin, L. Salvo, E. F. Rauch: Acta Mater. 54 (2006), 3801.
[6] K. Kubota, M. Mabuchi, K. Higashi: J. Mater. Sci. 34 (1999), 2255.
[7] B. Hadzima, M. Janecek, M. Bukovina, R. Kral: Int. J. Mat. Res. 100 (2009) 9, 1213.
[8] V. M. Segal: Mater. Sci. Eng. A197 (1995), 157.
[9] N. A Smirnova, V. I. Levit, V. I. Pilyugin, R. I. Kuznetsov, L. S. Davydova, V.A. Sazanova: Fiz. Met. Metalloved. 61 (1986), 1170.
[10] K. Kondoh, T. Aizawa: Mater. Trans. 44 (2003), 1276.
[11] R. Z. Valiev: Mater. Sci Forum 243-245 (1997), 207.
[12] C. C. Koch, Y. S. Cho: Nanostr. Mater. 1 (1992), 207.
[13] M. Furukawa, Z. Horita, M. Nemoto, T. G. Langdon: J. Mater. Sci. 36 (2001), 2835.
[14] Z. Horita, T. Fujinami, T.G. Langdon: Mater. Sci. Eng. A318 (2001), 34.
[15] S. R. Agnew, O. Duygulu: Mater. Sci. Forum 419-422 (2003), 177.
[16] A. Gholinia, P. B. Prangnell, M. V. Markushev: Acta Mater. 48 (2000), 1115.
[17] K. Matsubara, Y. Miyahara, Z. Horita, T.G. Langdon: Acta Mater. 51 (2003), 3073.
[18] Y. Miyahara, Z. Horita, T. G. Langdon: Mat. Sci. Eng. A 420 (2006), 240.
[19] E. Rauschnabel, V. Schmidt: Jour. Mat. Proc. Tech. 35 (1992), 371.
[20] R. Li, Z. Nie, T. Zuo: Mat. Sci. Eng. A 464 (2007), 28.
[21] M. R. Barnett, Z. Keshavarz, A. G. Beer, D. Atwell: Acta Mater. 52 (2004), 5093.
[22] T. Murai, S. I. Matsuoka, S. Myiamoto, Y. Oki: J. Mat. Proc. Tech. 141 (2003), 207.
[23] J. Bohlen, S. Yi, J. Swiostek: Scripta Mat. 53 (2005), 259.
[24] J. Mueller, S. Yi, M. Janecek, L. Wagner: Int. Jour. Mat. Res. 100 (2009), 838.
[25] E. D. McBride: J. Am. Med. Assoc. 111 (1938), 2464.
[26] M. S. Znamenskii: Khirurgiia 12 (1945), 60.
[27] M. Furukawa, Z. Horita, M. Nemoto, T. G. Langdon: J. Mater. Sci. 36 (2001), 2835.
[28] M. P. Staiger, A. M. Pietak, J. Huadmai, G. Dias: Biomater. 27 (2006) 9, 1728.
[29] Y. W. Song, D. Y. Shan, E. H. Han: Mater. Letters 62 (2008) 17-18, 3276.
[30] K. Y. Chiu, M. H. Wong, F. T. Wong, H. C. Wong: Surf. Coat. Tech. 202 (2007), 590.
[31] L. C. Li, J. C. Li, Y. Li: Surf. Coat. Tech. 185 (2007), 92.
[32] C. L. Liu, Y. C. Liu, X. B. Tian, P. K. Tian: Thin Solid Films 516 (2007), 422.
[33] F. Whitte, N. Hort, C. Vogt, S. Cohen, K. U. Kainer, R. Willumeit, F. Feyerabend: Curr. Opin. in Solid State and Mater. Sci. 12 (2008) 5-6, 63.
[34] T. Rzychon, A. Kiełbus: Mat. Sci Eng. 28 (2007) 8, 471.
[35] H. Friedrich, S. Schumann: Jour. Mat. Proc. Tech. 117 (2001), 276.
[36] A. Kiełbus, T. Rzychon, R. Cibis: J. Achiev. Mater. Manuf. Engin. 18 (2006), 135.

[37] L. A. Dobrzanski, T. Tanski, L. Cizek: J. Achiev. Mater. Manuf. Engin. 19 (2006), 49.
[38] T. Rzychon, A. Kiełbus: J. Achiev. Mater. Manuf. Engin. 28 (2007) 10, 601.
[39] B. R. Powell, V. Rezhets, M. P. Balogh, R. A. Waldo: JOM 54 (2002) 8, 34.
[40] A. S. Mohammadabadi, K. Dehghani: JMEPEG 17 (2008), 662.
[41] H. Conrad, J. Narayan: Scripta Mater. 42 (2000) 11, 1025.
[42] C. E. Carlton, P. J. Ferreira: Acta Mater. 55 (2007), 3749.
[43] C. S. Pande, R. A. Masumura, R. W. Armstrong: Nanstr. Mater. 2 (1993), 323.
[44] S. Takeuchi: Scripta Mater. 44 (2001) 8-9, 1483.
[45] H. Conrad, J. Narayan: Scripta Mater. 42 (2000) 11, 1025.
[46] R. Z. Valiev, Y. Estrin, Z. Horita, T. G. Langdon, M. J. Zehetbauer, Y. T. Zhu: JOM 58 (2006) 4, 33.
[47] K. Nakashima, Z. Horita, M. Nemoto, T. G. Langdon, Mater. Sci. Eng. A281 (2000), 82.
[48] S. Lee, T. G. Langdon: Mater. Res. Soc. Symp. Proc. 601 (2000), 359.
[49] M. Janecek, S. Yi, R. Kral, J. Vratna, K. U. Kanier: Int. Jour. Mat. Res. (2010), in press.
[50] D. G. Enos, Tech. Report 33 (1997) 2.
[51] B. Hadzima: PhD. thesis, University of Zilina (2003).
[52] Basis of Electrochemical Impedance Spectroscopy, Application note, http://www.gamry.com/App_Notes/EIS_Primer/EIS_Primer_2007.pdf, Gamry instruments, Warminster, PA, US (2007).
[53] F. U. Enikeev: Mater. Sci. Forum 243-245 (1997), 77.
[54] D. Landolt: Corrosion And Surface Chemistry Of Metals (2003).
[55] M. Bukovina, B. Hadzima, V. Skorik: Transfer Inovacii 15 (2009), 28.
[56] Y. Miyahara, Z. Horita, T. G. Langdon: Mat. Sci. Eng. 420 (2006) 1-2, 240.
[57] R. B. Figueiredo, T. G. Langdon: J. Mater. Sci. 43 (2008), 7366.
[58] Magnesium encyclopaedia, Corrosion behaviour, http://www.magnesium.com/w3/data-bank/index.php?mgw=217
[59] D. Song, A. Ma, J. Jiang, P. Lin, D. Yang, J. Fan: Corr. Sci. 52 (2010), 481.
[60] Ch. Schille, H.-P. Reichel, N. Hort, J. Geis-Gerstorfer: Magnesium 8 (ed. K. U. Kainer), WILEY-VCH, Weinheim, Germany, 2009, p 1195, ISBN 978-3-527-32732-4.
[61] J.-M Seitz, D. Bormann, J. Stahl, S. Schumacher, M. Kietzmann, S. Kramer, B. Schwab, T. Lenarz, Fr.-W. Bach: Magnesium 8 (ed. K. U. Kainer), WILEY-VCH, Weinheim, Germany, 2009, p 1189, ISBN 978-3-527-32732-4.
[62] A. Krause, N. v. d. Hoh, D. Bormann, Ch. Krause, Fr.-W. Bach, H. Windhagen, A. Meyer-Lindenberg: J. Mater. Sci. 45 (2010), 624.

7 Annex

The electronic version of this work is on enclosed DVD in PDF format.